2004-04-29

Ultrasonic Technique In Determination Of Grid-Generated Turbulent Flow Characteristics And Caustic Formation

Shangari B. Meleschi
Worcester Polytechnic Institute

ULTRASONIC TECHNIQUE IN DETERMINATION OF GRID-GENERATED TURBULENT FLOW CHARACTERISTICS AND CAUSTIC FORMATION

by

Shangari B. Meleschi

A Masters Thesis

submitted to the Faculty of the

WORCESTER POLYTECHNIC INSTITUTE

in partial fulfillment of the requirements for the

Degree of Master of Science

in

Mechanical Engineering

by

_____

Shangari B. Meleschi

April, 2004

Approved:

_____

Dr. William W. Durgin, Advisor

_____

Dr. Hamid Johari, Committee Member

_____

Dr. Zhikun Hou, Graduate Committee Representative

_____

Dr. David J. Olinger, Committee Member

_____

Dr. Tatiana A. Andreeva, Committee Member

Abstract

The present study utilizes the ultrasonic travel time technique to diagnose grid generated turbulence. Ultrasonic flow metering technology relies on the measurement and computation of small perturbations in the travel time of acoustic ultrasonic waves through the dynamic medium. The statistics of the travel time variations of ultrasonic waves that are caused by turbulence probably affect the performance of ultrasonic flow meters. Motivation for the study stems from the large travel time variations observed in typical ultrasonic flow and circulation meters.

Turbulent flow data was collected downstream of a grid introduced in a uniform flow in the wind tunnel using ultrasonic techniques. Grid turbulence is well defined in literature, and is nearly homogeneous and isotropic. The experimental investigation was performed under well-controlled laboratory conditions. The grid mesh sizes varied from 0.25-0.5in, and flow velocities from 0-20m/s. The ultrasonic transducers were of 100 kHz working frequency; and all of the data was collected with them oriented perpendicular to the mean flow. Path lengths were increased from 2-10in; and the data acquisition and control system featured a very high speed data acquisition card with an analog to digital converter that enabled excellent resolution of ultrasonic signals. Experimental data was validated by comparison to other studies.

The work aims to investigate the influence of the grid-generated turbulent flow on acoustic wave propagation, in terms of the variance of the travel time. The effect of turbulence on acoustic wave propagation was observed.

The experimental data was used to compute average travel times, acoustic travel time variances, and standard deviation amplitude fluctuations. The data was collected in the region estimated to be homogeneous and isotropic. Average travel time data support the assumption that only the large (as compared to the wavelength λ) turbulent inhomogeneities influence acoustic wave propagation. Variance data confirm the presence of a non-linear trend in the acoustic travel times with increasing path length. Amplitude fluctuations data confirm a correlation between areas of caustic formation and large amplitude fluctuations.

Acknowledgements

I would like to express my sincere thanks and appreciation to my advisor, Professor William W. Durgin. His confidence in my abilities to learn and be successful on the graduate level has inspired me to persevere, and strive for excellence. I will always be extremely grateful for his mentorship and financial support, without which my graduate education would not have been possible.

I would like to thank my entire committee Professor Zhikun Hou, Professor David J. Olinger, Professor Hamid Johari, and especially Dr. Tatiana A. Andreeva, who consistently contributed her knowledge, guidance, and friendship.

I would like to express my appreciation to the following people for their support: Barbara Furhman, Janice Dresser, Pam St. Louis, Gail Hayes, and Nancy Hickman.

I would like to thank Barbara Edilberti for all of her work and support on my behalf; her acts of kindness and friendship.

My sincere thanks are given to Jim Johnson, and Todd of the WPI Machine Shops, who worked above and beyond on my behalf.

My special gratitude to my girlfriend Farah for her love and support.

To my grandmother Alice, thank you for your life long believe in education and hard work. You continue to inspire me in life and in death.

And lastly, my very special thanks to my mother, Teresa, her faith in me, and unconditional love inspired me to work hard. I would not have been able to complete this work without her support.

List of Figures

Figure 1.1 Ultrasonic Flow Meter 3

Figure 1.2 Hybrid configuration for liquid level detection 5

Figure 1.3 Non-linear increase in the acoustic travel time variance with increasing non-dimensional length scale X/M 6

Figure 1.4 Ultrasonic Flow Meter Market Figures actual and projected for fiscal years 2002 & 2007 12

Figure 2.1 Mohamed & LaRue (1990) estimation of locally isotropic regions 17

Figure 2.2 Turbulent length scales 18

Figure 2.3 Hotwire probe 24

Figure 2.4 Basic Wheatstone bridge circuit of the hot film anemometer 24

Figure 2.5 Typical calibration curve, bridge voltage vs. mass flux 26

Figure 3.1 Ray geometry defining minimum travel path 38

Figure 4.1 AEROLAB wind tunnel 42

Figure 4.2 Pierre Curie (center), and Marie Curie (left) in their laboratory, awarded half of the Nobel Prize for Physics in 1903 45

Figure 4.3 6105-T5 Aluminum Extrusion Cross Section 47

Figure 4.4 Schematic of Linear Slide Rail Operation 48

Figure 4.5 Path length variation in perpendicular orientation 49

Figure 4.6 Spreader cross-section 49

Figure 4.7 Transducer Spreader Sub-Assembly 50

Figure 4.8 Complete Spreader Assembly 51

Figure 4.9 Transmitted Square Wave Burst Signal 54

Figure 4.10 Sent and received wave signals e_2 and e_1 respectively 55

Figure 4.11 Correlation of sent and received signals e_1 and e_2 56

Figure 4.12 Data Flow Diagram 57

Figure 4.13 Hardware Flow Diagram 58

Figure 4.14 Function Generator.vi 59

Figure 4.15 Gage Sample.vi 60

Figure 5.1 Ultrasonic supporting apparatus mounted to wind tunnel test section 64

Figure 5.2 Mean travel time vs. Non-dimensional length scale 0.25in grid 64

Figure 5.3 Magnified portion of Figure 5.2 66

Figure 5.4 Bar chart representation of mean travel time data 0.25in grid 67

Figure 5.5 Mean travel time vs. Non-dimensional length scale 0.25in grid 68

Figure 5.6 Magnified portion of Figure 5.5 69

Figure 5.7 Bar chart representation of mean travel time data 0.5in grid 70

Figure 5.8 Mean travel time vs. Non-dimensional length scale 1in grid

Andreeva and Durgin (2003) 71

Figure 5.9 Kravtsov (1968) description of wave propagation through a random medium

72

Figure 5.10 Amplitude standard deviations 73

Figure 5.11 Travel time variance 0.25in grid experiment 75

Figure 5.12 Travel time variance 0.5in grid experiment 76

Figure i CSScope.vi & Gage Sample.vi 85

Figure ii Wind tunnel test section and experimental apparatus 90

Figure iii (left to right) Function Generator and Oscilloscope 91

Figure iv Close-up of supporting apparatus 92

List of Tables

Table 5.1 0.25in grid mean travel time table 65

Table 5.2 0.5in grid mean travel time table 68

Table of Contents

LIST OF FIGURES

LIST OF TABLES

CHAPTER 1. INTRODUCTION **1**

1.1 History of Ultrasonic Flow Metering 1
1.2 Review of Sound Propagation through Random Media 8
1.3 Review of Ultrasonics & Ultrasonic Flow Metering Methods 11
1.4 Objectives and Methods 13

CHAPTER 2. FLOW CHARACTERISTICS **15**

2.1 Isotropic Turbulence 15
2.2 Flow Development and Determination of Local Isotropy 21

CHAPTER 3. WAVE PROPAGATION THROUGH RANDOM MEDIA **29**

3.1 Characteristics of Wave Behavior 29
3.2 Ray Theory and Statistics 31
3.3 Kolmogorov's "2/3" Law and Resulting Travel Time Equations 35
3.4 Fermat’s Principle 37
3.5 Caustics 39

CHAPTER 4. EXPERIMENTAL APPARATUS **41**

4.1 Wind Tunnel 41
4.2 Grid Fixture & Resulting Grid Turbulence 44
4.3 Ultrasonic Measurement System 45
4.4 Temperature Monitoring Controls 52
4.5 Data Acquisition System 52
4.5.1 Acquisition System Hardware 53
4.5.2 Acquisition System Software 58

CHAPTER 5. EXPERIMENTAL RESULTS AND DISCUSSION **61**

5.1 Travel Time Ultrasonic Techniques for Data Acquisition 61
5.2 Travel Time Fluctuations based on Ultrasonic Path Length 63
5.3 High Amplitude Standard Deviation & Caustic Occurance 71
5.4 Travel Time Variance & Caustic Occurance 74

CHAPTER 6. CONCLUSIONS AND RECOMMENDATIONS 78

6.1 Summary and Conclusions 78
6.2 Recommendations 80

BIBLIOGRAPHY 82

APPENDIX A. COMPUSCOPE 82G SOFTWARE INTERFACE 85

APPENDIX B. IMSL FORTRAN SIGNAL CORRELATION PROGRAM 86

APPENDIX C. PHOTOGRAPHS OF EXPERIMENTAL APPARATUS 90

Chapter 1. Introduction

1.1 History of Ultrasonic Flow Metering

As adolescents we all developed a fear of bats, associating them with unworldly monsters, while at the same time admiring their ability to navigate their nocturnal surroundings with little or no visibility. Perhaps one of the best examples of acoustic sensing in nature is echolocation; the process by which bats send out sound waves using their mouths or nose, and retain detailed information about their surroundings from the sound of the echo. In a similar fashion, acoustic waves can be used for flow diagnostics to collect information and data pertaining to the traversed medium. Ultrasonic flow metering, for example, given comparable fundamentals, is the process by which acoustic waves within the ultrasonic frequency range from 20 kHz to 2.45MHz are used to measure volumetric flow rates in pipelines.

Ultrasonic waves, or very high frequency acoustic waves, in liquids and solids have been used for many measurement applications including sonar, electrical filters, nondestructive testing, and medical instrumentation (Ristic, 1983). Two techniques, Doppler and transit time (Δt); have been used for flow measurement during the last century (Lynnworth, 1989). Early pioneers in the field include Herrick (1977), Chilowsky (1932) with his contributions for Doppler, and Rütten with his patents pertaining to transit time methods. Variations of the transit time of flight ultrasonic flow meter can also be traced back to the late R.C. Swengel, both a ham radio operator and inventor, who around 1947 or 1948 was able to obtain favorable results from his early

flow metering instrumentation in water. From the contributions of Swengel and others, ultrasonic flow metering technology has been developed over the past fifty plus years, and has evolved to support some of the most popular and efficient flow measurement devices available today. The non-invasive nature of ultrasonic flowmetering makes it highly applicable to oil and gas pipeline measurement systems, feedwater flow measurement, as well as a plethora of other areas where other types of flow meters are not appropriate due to their intrusiveness or associated pressure loss. Ultrasonic technologies have also been applied to oceanographic current sensors, interface sensors in beverage bottling plants, thickness monitors to control chemical depositions and etching, and arterial diagnostic systems to track blood flow throughout the body. As such, some of the more prominent benefits of ultrasonic systems include noninvasiveness, ease of operation and installation, fast response to flow variations, increased time between calibrations, and the modular design and interchangeability of components enabling rapid system repair. Not exclusive to the private sector, these ultrasonic devices can also be found in a domestic setting, utilized in hot water and methane metering systems used to monitor water and gas usage in large housing developments.

Ultrasonic transducers, the active elements in an ultrasonic flow meter, have two main functions: transmission and reception. Depending on the device and its purpose, there may be multiple transducers for each function, or a single transducer for all functions (Papadakis, 1999).

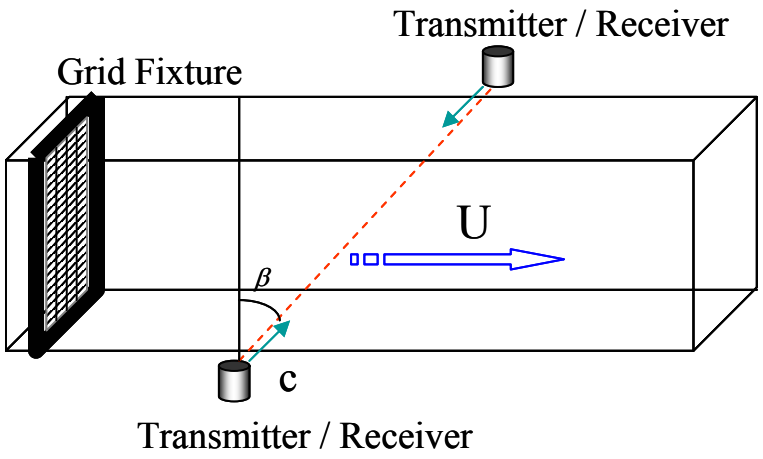

Figure 1.1 - Ultrasonic Flow Meter

The most common of the ultrasonic flow meters in use today can be categorized into three categories; clamp-on, wetted, and hybrid. The utility of clamp-on meters is often the deciding factor in choosing an ultrasonic measurement system. Clamp-on flow meters, for example, can be installed without modifications to the metered channel or pipe, thus eliminating the need to empty or depressurize an area to allow for a sensor to be installed. For smaller diameter pipes, sensors can easily be positioned for measurement by an operator irregardless of skill level (Lynnworth, Mágori, 1999). Additionally, the often corrosive nature of internal sensors that remain in constant contact with the diagnosed fluid, adds considerable weight to an argument for using non-invasive instrumentation.

For example, to avoid water shortages and decreased water pressure, a removable transducer could be attached near the bottom of a water tower to monitor water levels. As the water supply diminished, the ultrasonic metering system might trigger pumps to replenish the supply back to acceptable levels. In this case, possible contamination of the

water supply by an invasive flow metering element may warrant the use of a clamp-on meter.

Although often effective solution, not all situations are conducive to the application of a clamp-on meter. In these cases the sensors or transducers utilized in the ultrasonic flow meter are of a *wetted* type, denoting there contact with the fluid. As such, *wetted* ultrasonic flow meters are integrated into the larger system much like conventional metering devices. For example, liquid presence detecting at a discrete point, based on detecting an echo from the far wall of a large liquid filled storage tank; sensing the change in ring-down when the probe is slid up and down the vessel wall to determine the fluid level; sensing change in rind-down at a fixed point when the level passes through that point; sending the sound wave vertically up through the liquid column and timing the round-trip (Lynnworth, Mágori, 1999). Figure 1.2 illustrates an example of a liquid level sensing arrangement using ultrasonic sound waves for a large fluid filled storage tank.

Combining the operational advantages of both the clamp-on and wetted types of transducers yields a *hybrid* type of meter. In this configuration, a wetted plug touches the fluid but the ultrasonic transducer is external, touching only the dry side of the plug, and removable at any time because physically only the plug is a permanent part of the pressure boundary (Lynnworth, Mágori, 1999). For example, a variation on the *wetted* configuration described above for liquid level sensing inside a storage tank could be converted to a *hybrid* type arrangement by placing the transducer outside of the vessel, with a reflector present inside the tank instead, thus isolating the transducer from direct contact with the fluid.

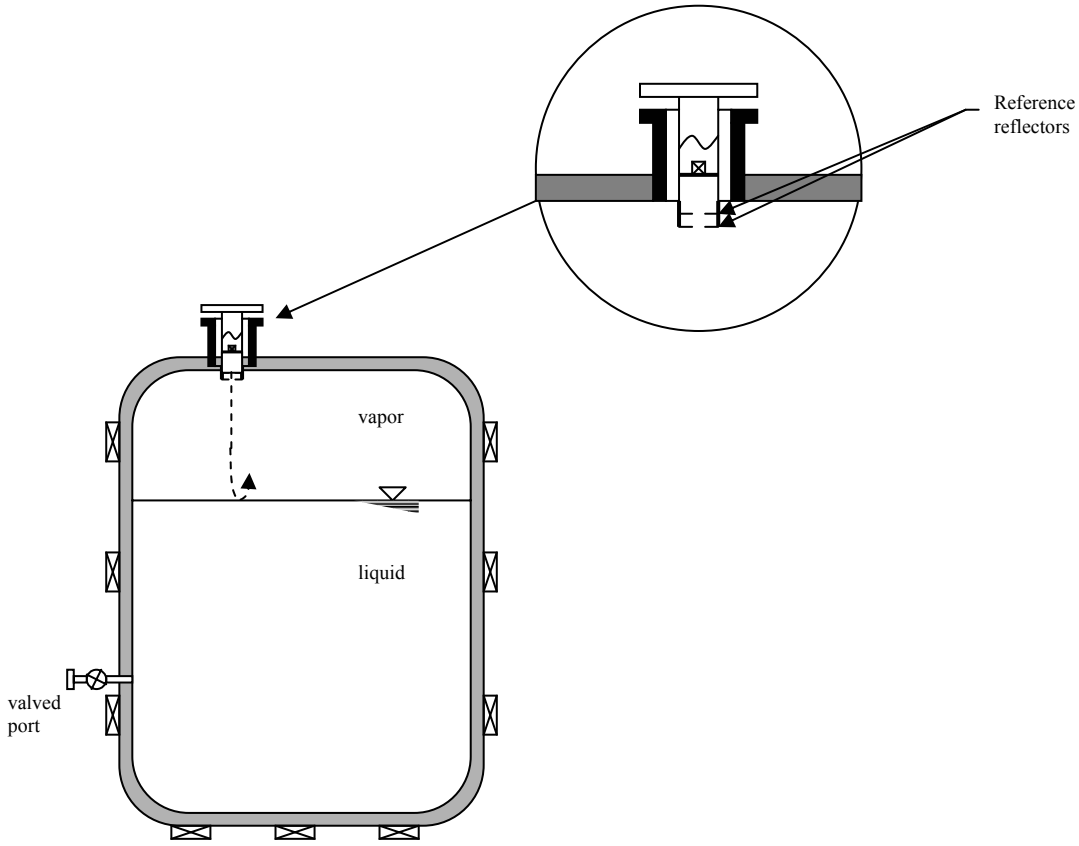

Figure 1. 2 – Hybrid configuration for liquid level detection

Given the abundance of operational, and process monitoring advantages to using an ultrasonic flowmeter as opposed to conventional mechanical metering techniques, one might inquire as to why the bulk of the flow meters in service were not of ultrasonic design. There are limiting factors which inhibit the use of these ultrasonic devices, many of which stem from the fluctuating dynamic conditions of the probed medium. Despite the advances in computing capabilities and subsequent improvements in measuring travel-time, ultrasonic flow meter accuracy has not improved very much at all. The explanation may be linked to the effect of turbulence on ultrasonic waves, primarily fluctuations in velocity and density (Andreeva, 2003). *Andreeva* examined, in detail, the

effects of a grid-generated turbulence on ultrasonic measurements, while restructuring the basic ultrasonic flow meter equation to account for the effects of turbulent velocity and sound speed fluctuations. The latter investigation was spawned from earlier experimental work by *Weber* (1994) that utilized the ray trace method to examine the effects of turbulent flows on sound waves propagation through a velocity field (Andreeva, 2003). Specifically, it was found in these studies that turbulence could result in substantial inaccuracy of volumetric flow measurements.

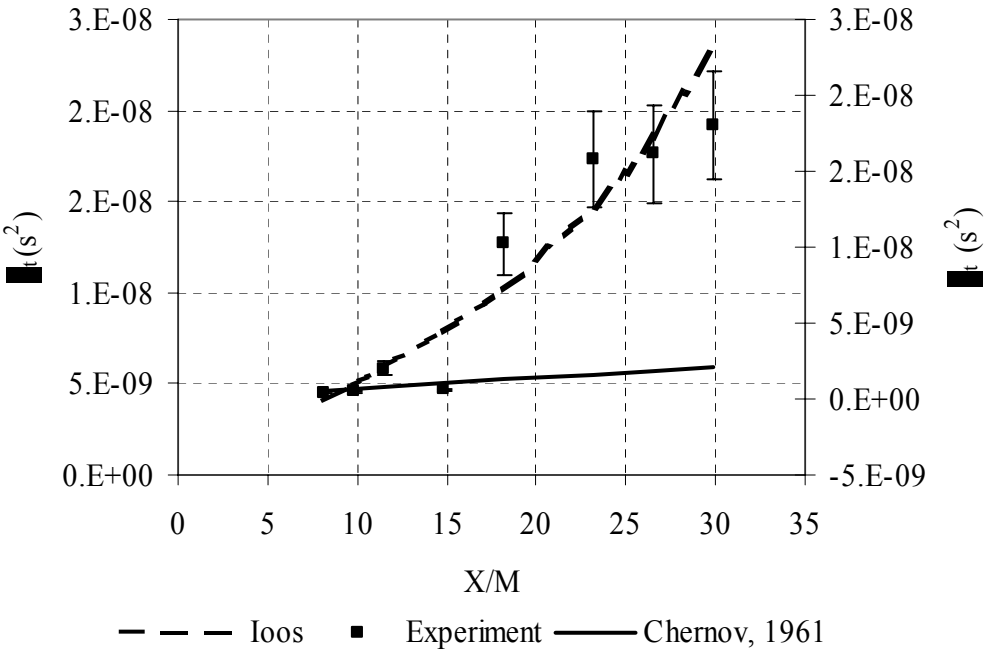

Figure 1-3 – Non-linear increase in the acoustic travel time variance with increasing non-dimensional length scale X/M.

There are, of course, a large number of phenomena that effect transit time and, therefore, accuracy. The focus of this investigation will revolve around the effects of turbulence that contributes to a non-linear trend in the acoustic travel time variance. Figure 1-3 shows the theoretical predictions of Chernov (1960) and Iooss (2000) and

measurements made by Andreeva (2003). The acoustic travel time variance exhibits a linear increase for small values of x/M, where "x" is the ultrasonic path length, and "M" the grid mesh size. However, for large x/M the acoustic travel time variance data increases and follows a non-linear trend, as illustrated in Fig. 1.3.

Second, the design of the acoustic travel time experiment is such that it allows us to examine the relationship between turbulent intensity and ultrasonic path lengths with regard to the acoustic travel time variance. As the ultrasonic path lengths increase and/or the characteristic grid mesh sizes decrease, the likelihood of a specific acoustic phenomenon called the caustics occurring, increased. Basically, ultrasonic waves actually converge on two-dimensional surfaces or planes in a three-dimensional volume called caustics, which can be described as a region on which two or more rays coalesce, producing high intensities. High acoustic intensities cause sound speed changes and spawning of upper and lower side bands so that the variability of the travel time increases.

These caustics thus, contribute to the scattering of the ultrasonic wave and overall variance of travel time with consequent error in the flow metering system. Considering that our analysis is based upon time of flight calculations, formulation of these acoustic disturbances is of paramount importance. In this work, we seek to verify, experimentally, that the higher the turbulent intensity, the shorter the distance at which the first caustics may occur.

Acoustic travel time data obtained experimentally which describes the non-linear trend in the acoustic travel time variance will be compared to preliminary findings by *Durgin*, *Andreeva* and *Meleschi* (Andreeva, et al. 2004) illustrated in Fig. 1.3. A

correlation between these preliminary findings and the data present herein, serves to validate our findings and support theoretical predictions of a non-linear increase in the acoustic travel time variance.

Given the background information presented pertaining to ultrasonic flow metering, a brief description of how sound propagates through random mediums is presented in the following.

1.2 Review of Sound Propagation through Random Media

Throughout the last half of the last century, technological advances in understanding how turbulence influences sound wave propagation have facilitated the continued development of improved ultrasonic devices for flow measurement. The scattering of sound waves in turbulent flows was first considered by Obukov in 1941; subsequently other authors have devoted papers to the same problem (Tatarski, 1961). Specifically, Tatarski (1961), as well as Ishimaru (1978) and Chernov (1960), include a wide variety of experimental and analytical data relating to wave propagation through the earth's atmosphere and other relevant flows.

Atmospheric studies of electromagnetic and acoustic wave propagation were pertinent to radio physics, and attracted the attention of many investigators given their connection with the long distance propagation of V.H.F. and U.H.F. radio waves by scattering in the ionosphere and troposphere (Tatarskii, 1961). The turbulent state of the atmosphere promotes fluctuations in the refractive index of air. Sound propagation is sensitive to these random variations in the effective refractive index, which fluctuates as a

function of temperature and velocity. *Di Iorio and Farmer* showed that these medium velocity fluctuations can be a dominant source of acoustic scattering (Andreeva, 2003). Similarly, observations of sound wave propagation through temperature gradients confirm their impact on the refractive index and subsequent acoustic scattering. The index of refraction *n* of the earth's atmosphere, specifically in the troposphere (height < 17kn), is given by (Ishimaru, 1978):

$$n-1=\frac{77.6}{T}(P+4810e/T)\times 10^{-6} \tag{1.2.1}$$

whereas T denotes the absolute temperature expressed in degrees Kelvin, P the pressure in millibars, and e the water vapor pressure in millibars. Thus, the problem of wave propagation and turbulence is one of the important problems in the areas of radio physics, atmospheric optics and acoustics" (Tatarskii, 1960) at large. Moreover, these atmospheric studies are of particular interest to our investigation in that the naturally occurring turbulent flow characteristics are comparable to those artificially maintained in the wind tunnel.

Although a large emphasis was placed on conducting outdoor experiments for atmospheric observations and measurements, these studies inherently featured a large degree of uncertainty in characterizing the surrounding environment especially turbulence. Physical parameters which describe these mediums, namely velocity and temperature, were not obtained exclusively, making it difficult to assess their individual contributions to the resulting acoustic wave behavior. However, because the nature of these environments are not well controlled, studies conducted within the turbulent or thermal field produced by a grid or jet in the laboratory may be more appropriate in

modeling an open air environment to examine how sound is influenced by turbulence (Benon, Juvé, Comte-Bellot, 1990).

Numerical techniques for simulating acoustic wave propagation through a turbulent medium were introduced by Benon, Juvé, Comte-Bellot circa 1941 in their studies relating to phase variance and the travel-time variance of acoustic waves moving through a random inhomogeneous medium. In generating their turbulent field, grid generated flows 40 grid-mesh lengths downstream were considered quasi-isotropic and in spectral equilibrium. Likewise, their spectral forms are comparable; and their statistical properties should only differ by a length scale L_o, and a turbulence level described by:

$$u_1' = \sqrt{\overline{u_1^{\,2}}}, \; u_1 \tag{1.2.2}$$

corresponding to the fluctuating velocity component in the x_1 direction. In addition an adapted von Karman spectral model for incompressible, isotropic turbulence was used to generate the simulated fields.

The ray tracing method was employed to simulate the actual movement of the acoustic wave. An initial position and direction of propagation of the acoustic wave front was assumed, and a point reference established thereon was used to follow the wave's trajectory through the velocity field. In these simulations the transit times of the acoustic waves were considered to be small compared to the time scales of the simulated velocity fluctuations. Consequently, a "frozen" field treatment was adopted, descriptive of the static condition of the velocity field as observed in the frame of reference of the propagating wave. Effective application of the ray tracing method is presented at length in the papers of Andreeva (2003), and Webber (2004).

1.3 Review of Ultrasonics & Ultrasonic Flow Metering Methods

It's is now over a decade since the Trans Alaska Pipeline (TAP) went into operation, an oil pipeline that runs 800 miles from wells at Prudhoe Bay to the port of Valdez. The pipeline's flow sensor used in the leak detection system is an ultrasonic flow meter, developed by the Oceanic Division of Westinghouse Electric Corporation (Lynnworth, 1989). At present, the worldwide Ultrasonic Flow-metering market is expected to grow at a compound annual growth rate of 7.9% over the next 5 years. Evidence of ultrasonic technology's value to industry as effective flow diagnostic solutions can be taken from Fig 1.4 which illustrates the Ultrasonic Flow Metering market size quoted in 2002 at nearly $406 Million dollars, is projected to expand to a $600 million dollar industry by 2007.

Transit time flow metering equipment is currently available from a relatively small number of vendors, with their applications primarily geared towards liquids over a wide range of operating temperatures. Ultrasonic flow diagnostic equipment was developed based upon the analysis of time of flight calculations for ultrasonic waves that traverse the mean flow of the probed medium. As these acoustic waves move through the probed medium, they inherently acquire information pertaining to their traveled paths. The exact instance that each ultrasonic wave is transmitted and then received is used to compute an acoustic travel time.

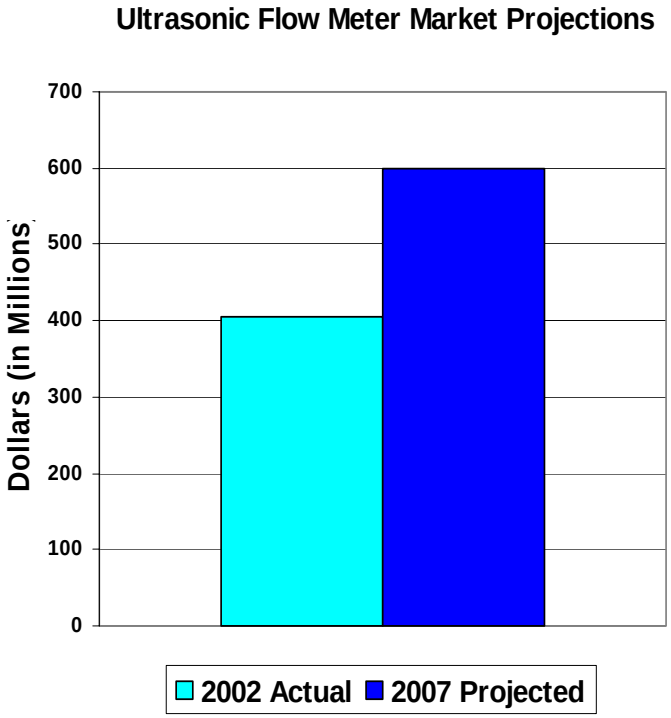

Figure 1.4 - Ultrasonic Flow Meter Market Figures actual and projected for fiscal years 2002 & 2007

Information relating the traveling waves and the probed environment such as temperature, density, velocity, and traversed distances, etc. can be solved for explicitly using the relevant equations governing wave propagation. Typical accuracies for these instruments are on the order or 0.5%, with response times as short as 1 millisecond. Limits on performance and accuracy of ultrasonic travel time systems are imposed by factors that perturb the propagation of the transmitted signal. Specifically, anomalies such as gas bubbles or any other body that promotes scattering of the traveling waves, turbulence, acoustic interference, and signal jitter, etc.

1.4 Objectives and Methods

The primary goal of this thesis is to apply the travel time ultrasonic technique for data acquisition over the span of a grid-generated turbulence produced in the wind tunnel. Experimentally, we seek to observe the non-linear behavior of the acoustic travel time variance as it relates to changes in the turbulent intensity, velocity, and distance. Furthermore, the experimental design, consisting of two transducers positioned perpendicular to each other ($\beta = 0$), is such that the statistics of the collected data should confirm:

1. A non-linear increase the acoustic travel time variance predicted by Iooss (2000) at some propagation distance related to the occurrence of the caustics.
2. Theoretical and numerical investigations which predict that the greater the turbulent intensity, the shorter the distance needed to observe wave interaction and formation of caustics (i.e. non-linear trends in the travel time variance will appear at shorter propagation distances).

The body of this thesis is organized as follows. In Chapter 2 we review the defining flow characteristics of isotropic and grid-generated turbulence. In Chapter 3 we present the fundamental equations regarding wave propagation through random media, and highlight relevant works in the study of acoustic wave behavior. In Chapter 4 we present a description of our experimental apparatus and supporting data

acquisition systems. The collected and analyzed data is presented in Chapter 5, along with a discussion of our experimental findings and comparisons to similar studies. Conclusions and our aspirations for future research are outlined in Chapter 6.

Chapter 2. Flow Characteristics

2.1 Isotropic Turbulence

For a viscous fluid there are two distinct states of motion: laminar and turbulent. For example, a fluid passes through a pipe of diameter *l* with an average velocity *v*, through flow visualization using coloring dye we can observe that at low velocities, the streamline is smooth and clearly defined. These conditions are characteristic of a laminar flow. However, at increased velocities, the streamline is no longer smooth and the fluid undergoes irregular and random motion (Ishimaru, 1978). The latter is indicative of a turbulent flow. Under turbulent fluid motion various quantities show a random variation with time and space coordinates. Thus, it is an irregular condition of flow such that statistically distinct average values can be discerned (Hinze, 1959). In cases where the turbulence has the same structure in all parts of the flow field, quantitatively, the turbulence can be defined as homogeneous. Furthermore, the turbulence is classified as isotropic if its statistical features do not change with position throughout the flow, so that perfect disorder resigns (Hinze, 1959).

We use isotropic turbulence because it is the most easily characterized and is well defined in the literature. A grid is a convenient way to make isotropic turbulence. Thus, for our purposes we are primarily concerned with the underlying physical characteristics of grid-generated turbulence. Comprehensive reviews of homogeneous and isotropic turbulence are presented by Batchelor (1953), Hinze (1959) and Monin & Yaglom (1975) (Mohamed, LaRue, 1990). Additionally, information regarding specification of areas of

isotropy in grid-generated turbulent flows is presented by Mohamed & LaRue (1990), and Corrsin et al (1980). From the aforementioned, it can be shown that the flow becomes nearly locally isotropic, isotropic and homogeneous starting at about y/M equal to 25, 40, 50, and 55 for Re_{mu} = 6000, 10000, 12000 and 14000 respectively (Mohamed et al., 1990), where y denotes the distance downstream of the grid and M the grid mesh size. These positions are taken to correspond to the beginning of the decay power law region, and are in agreement with previous data sets of Corrsin (1963). A plot of these projected areas of isotropy is illustrated in Fig. 2.1, which relates Reynolds mesh number, Re_{mu} to y/M. Calculation of our Reynolds mesh numbers yielded similar values: Re_{mu} = 5999, 9857, 12428 and 13714 respectively for the same y/M. Thus, applying a best fit line to the Mohammed & LaRue (1990) data, and extending the trend line to higher values of y/M, we define the distance y downstream of the grid which is approximately homogeneous and isotropic. As such, the data was collected at approximately 27-33" inches downstream of the grid.

Paradoxically, the unique characteristics of grid turbulence violate the definition of the media because it is not self-sustaining. For example, to generate grid turbulence, a grid of (say) circular rods is placed perpendicular to a uniform flow stream. After a certain distance, a homogenous, isotropic field of turbulence is achieved as the vortices generated by the cylinder interact (Panton, 1996). Thus, to a large extent the turbulent flow within the test section can be classified as isotropic. The streamwise evolution of a temporally stationary turbulence field produced by a grid placed in stream of a steady uniform duct flow holds a strong resemblance to the time evolution of the mathematical ideal of isotropic turbulence.

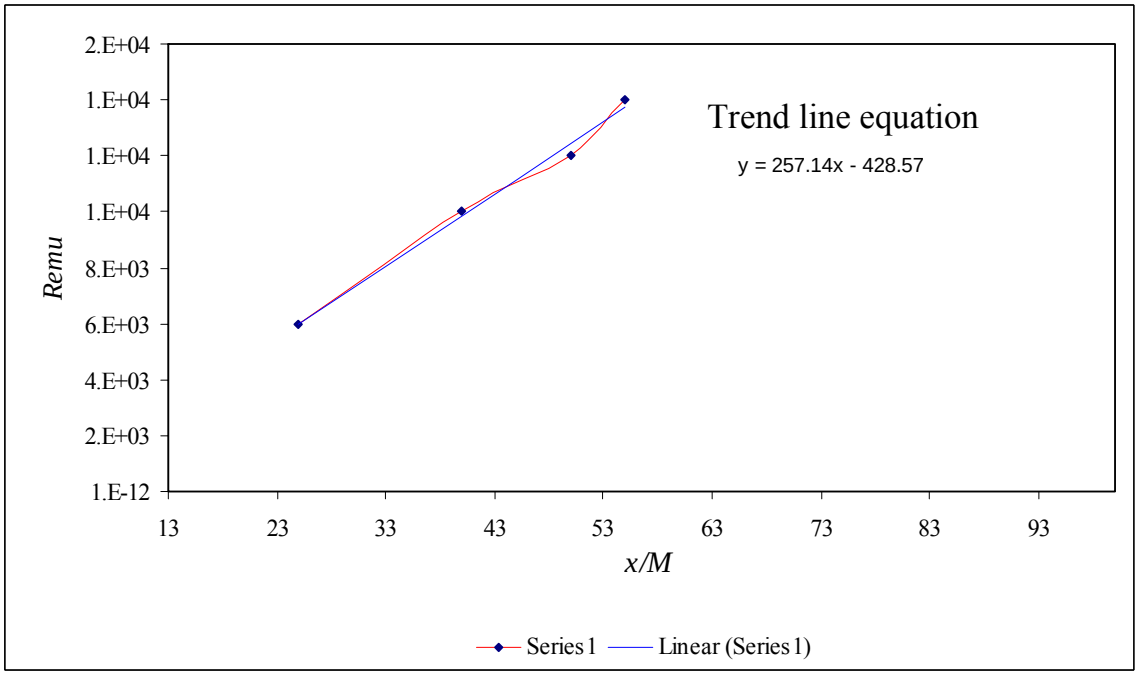

Figure 2-1 - Mohamed & LaRue (1990) estimation of locally isotropic regions

This was first observed by Simmons & Salter (1934) (Comte-Bellot, Corrsin, 1971). Thus, from these observations, we know that a practically isotropic turbulence can be produced by means of grids placed in stream of a uniform flow (Hinze, 1959). However, as the turbulence decays with increasing distance moving away from the grid, the Reynolds number will decrease, and so the character of the turbulence will change as well (Hinze, 1959). Although the characteristics and behavior of isotropic turbulence are well documented and understood, true isotropy is never realized by any turbulent flow. Rather, turbulent flow conditions can be controlled to facilitate a flow that more or less approaches isotropy with a high degree of similarity.

The characteristics of turbulent flows, usually irregular fluctuations in velocity, are observed in all three spatial dimensions (Panton, 1996). While tracking changes in

velocity at a fixed point in a flow, the time history of the fluctuations at first glance resembles a random signal. However, there is structure to these fluctuations; thus, it is not accurate to classify them as random (Panton, 1996).

Irregularities that are observed in the velocity field are frequently envisioned as eddies. These eddies are the building blocks of turbulence, so to speak, and are generated in large and small sizes, often one on top of another and even one inside of the other (Ishimaru, 1978).

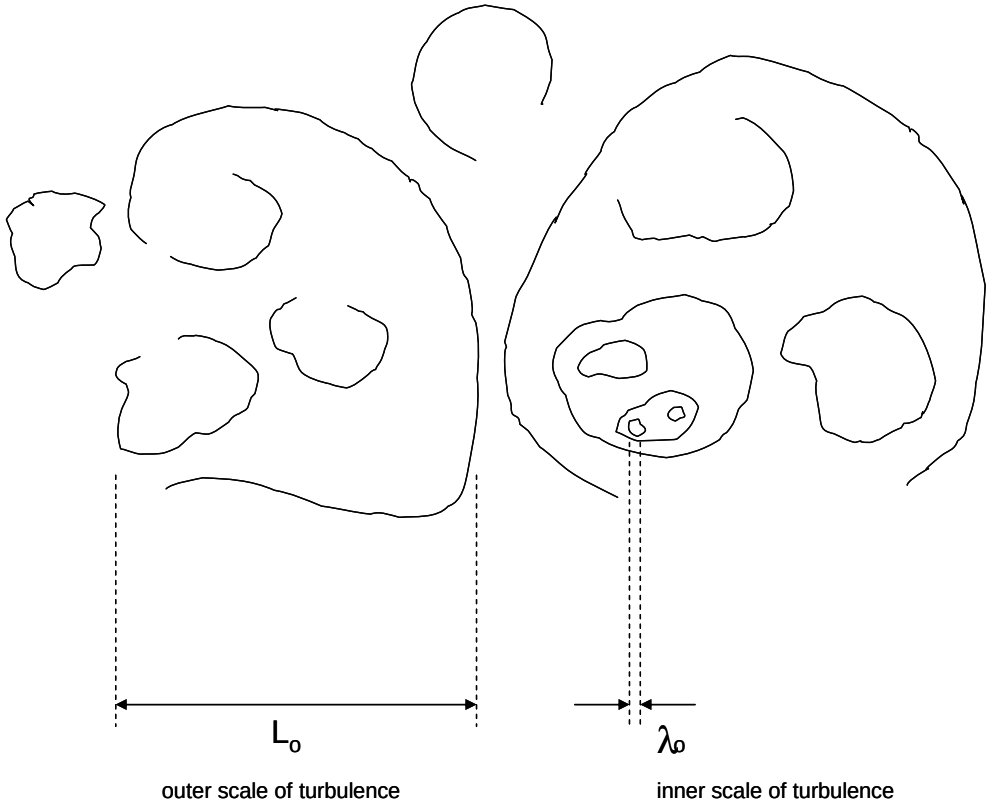

Figure 2-2 - Turbulent length scales

By Kolomogorov (1941), variations in the average velocity cause energy to be introduced into turbulence (Ishimaru, 1978). Following Ishimaru (1978), we can estimate

eddy sizes as illustrated in Fig. 2.2. For example, the turbulent eddies that are produced in the atmosphere differ from those produced closer the earths surface due to the varying horizontal wind velocities dependence on altitude. Thus, the resulting turbulence will be of a size approximately equal to the determined height. This size is called the outer scale of turbulence and is designated by $L_{o,}$ corresponding to the size at which the energy enters into the turbulence (Ishimaru, 1978). Eddies that are of the order greater than Lo generally are anisotropic. Naturally, eddies of smaller sizes compared to L_o are generally isotropic. From this relationship, we find that the kinetic energy per unit mass per unit time and the energy dissipation per unit mass per unit time is approximately on the order of:

$$V_o^3 / L_o \tag{2.1.1}$$

$$\nu V_o^2 / L_o^2 \tag{2.1.2}$$

where V_o denotes the velocity associated with eddies of the order of L_o, and ν the kinematic viscosity (Ishimaru, 1978). In these cases since the Reynolds number is considerably large, the kinetic energy is sufficiently larger then the dissipative. Physically, the bulk of this kinetic energy may be transferred to smaller eddies. Thus, given velocities $V_1, V_2, \ldots, V_n$ corresponding to eddies of sizes $L_1, L_2, \ldots, L_n$ the kinetic energies per unit mass per unit time for eddies of all sizes can be expressed as:

$$V_o^3 / L_o \cong V_1^3 / L_1 \cong V_2^3 / L_2 \cong V_3^3 / L_3 \cong \ldots \cong V_n^3 / L_n \tag{2.1.3}$$

As the size of the eddies get smaller and approach the lower limit l_o, the dissipation

$\nu V_o^2 / L_o^2$ increases until it is on the same order as the kinetic energy dissipation ε, which can be expressed as:

$$V_o^3 / L_o \cong V_1^3 / L_1 \cong \ldots \cong V_l^3 / l_o \cong \upsilon V_l^2 / l_o^2 \cong \varepsilon \tag{2.1.4}$$

At this size l_o, all the energy is dissipated into heat and practically no energy is left for eddies of size smaller than l_o. Thus, this size l_o is called the inner scale, or Kolmogorov scale, of turbulence (Ishimaru, 1978). In our experiment, the inner turbulent micro scales for the ¼ and ½ inch grids were approximately 6mm and 12mm respectively. The parameter ε present in equation (2.1.4) above denotes the energy dissipation rate. Thus, we determine that for eddies falling within the upper and lower limits L_o and l_o respectively, the velocity V can be related to the energy dissipation rate ε by:

$$V \sim (\varepsilon L)^{1/3} \tag{2.1.5}$$

From equation (2.1.5), the form of the structure function for the velocity fluctuation can be derived and is expressed as:

$$D_v(r) = C(\varepsilon r)^{2/3} \tag{2.1.6}$$

for,

$$l_o << r << L_o \tag{2.1.7}$$

where the quantity C is a dimensionless constant (Andreeva, 2003). Equation (2.1.6) is known as the "two-thirds law" which was first formulated by Kolmogorov and Obukhov.

2.2 Flow Development and Determination of Local Isotropy

As described by Monin & Yaglom (1975), the flow downstream of a grid can be divided into three regions. The first region is nearest the grid, and is the developing region of the flow where the rod wakes merge. The flow is this region is inhomogeneous and anisotropic, consequently producing turbulent kinetic energy. In the second region that follows, the flow is nearly homogenous, isotropic and locally isotropic where there is appreciable energy transfer from one wave number to another. The third and last region of decay encompasses the area furthest downstream from the grid where viscous effects act directly on the largest energy containing scales. These three regions of turbulent generation and decay are important is assessing the applicability of the decay power law.

The decay power law, only valid in the second region as outlined above, and often referred to as the power-law region, is applied to determine quantitatively the expected areas of isotropy downstream of the grid. In an isotropic flow, the skewness of the velocity, as described by:

$$S(u) = \overline{u^3} \Big/ \overline{u^2}^{\frac{3}{2}} \tag{2.2.1}$$

has a zero value. Furthermore, Batchelor (1953) showed that the skewness of the velocity derivative, as described by:

$$S(\partial u/\partial x) = \overline{(\partial u/\partial x)^3} \Big/ \overline{((\partial u/\partial x)^2)}^{\frac{3}{2}} \tag{2.2.2}$$

should be a constant in the isotropic region. Thus, the point where the skewness of the velocity derivative becomes constant can be estimated as the position where the flow is locally isotropic.

Perhaps a third indicator of isotropic positions downstream of the grid is achieved through a comparison of the dissipation rate of turbulent kinetic energy (Mohamed, LaRue, 1990). In the region downstream of the grid that is nearly homogeneous and isotropic, the turbulent energy equation is expressed as:

$$\varepsilon^*_u = -\frac{1}{2}\frac{d\overline{q^2}}{dt} \tag{2.2.3}$$

where,

$$\overline{q^2} = (\overline{u^2} + \overline{v^2} + \overline{w^2}) \tag{2.2.4}$$

From Taylor's (1935) hypothesis, and assuming the decay power law region is indeed homogeneous and isotropic we satisfy the following condition, and thus the turbulent energy equation as presented above in Eq. (2.2.3) is rewritten as:

$$\overline{u^2} \approx \overline{v^2} \approx \overline{w^2} \tag{2.2.5}$$

$$\varepsilon^*_u = -\frac{3}{2}U\frac{d\overline{u^2}}{dx} \tag{2.2.6}$$

where $d\overline{u^2}/dx$ is computed directly from the plot relating $\overline{u^2}$ and x/M_u. However, near the grid this form of the turbulent kinetic energy equation is not realistic introducing considerable error, and thus a third variation of the equation is written as expressed in Eq. (2.2.7) below.

$$\varepsilon_u = \frac{15\nu}{U^2}\overline{\left(\frac{\partial u}{\partial t}\right)^2} \tag{2.2.7}$$

This equation is an independent estimate of the dissipation rate, ε_u as obtain from the assumption of local isotropy, the measured time derivative of the velocity downstream of the grid, and Taylor's hypothesis. However, the expression for ε^*_u as presented in Eq. (2.2.6) is based both on the assumptions of isotropy and homogeneity. Thus, at downstream distances far enough from the grid where the flow is taken to be nearly homogeneous, isotropic and locally isotropic, the ratio of the two dissipation rates as expressed in Eq. (2.2.8), should be nearly unity (Mohamed, LaRue, 1990).

$$\varepsilon_u \Big/ \varepsilon^*_u \cong 1 \tag{2.2.8}$$

Experimentally, regions of isotropy can be determined through hot wire anemometry. A hot-wire probe, can be used to measure the fluctuating velocity, as conducted by Mohamed, et al (1990). The electronic circuitry supplies the applied voltage needed to sustain a constant probe temperature while immersed in the mean flow and subject to cooling by convection. Analytically, there is a relationship between the fluctuation of these bridge voltages over time and the corresponding velocity fluctuations in the flow stream.

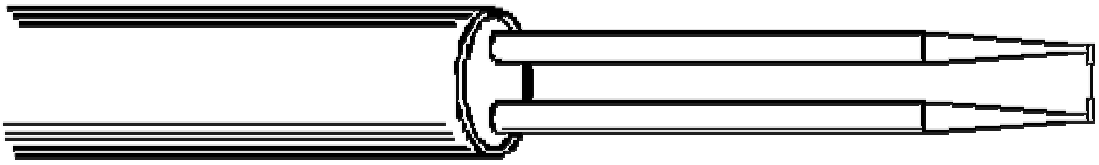

Figure 2-3 - Hot wire probe

The actual hot film sensor that measures the flow velocity is a small cylindrical element, on the order of a few microns, mounted between two stainless steel fingers as illustrated in Fig. 2.3. The sensor becomes one of the resistive elements in a four- corner Wheatstone bridge circuit as shown in Fig. 2.4. The circuit heats the sensor to a constant temperature by adjusting the power dissipated in the sensor such that its resistance, and hence temperature, remains constant.

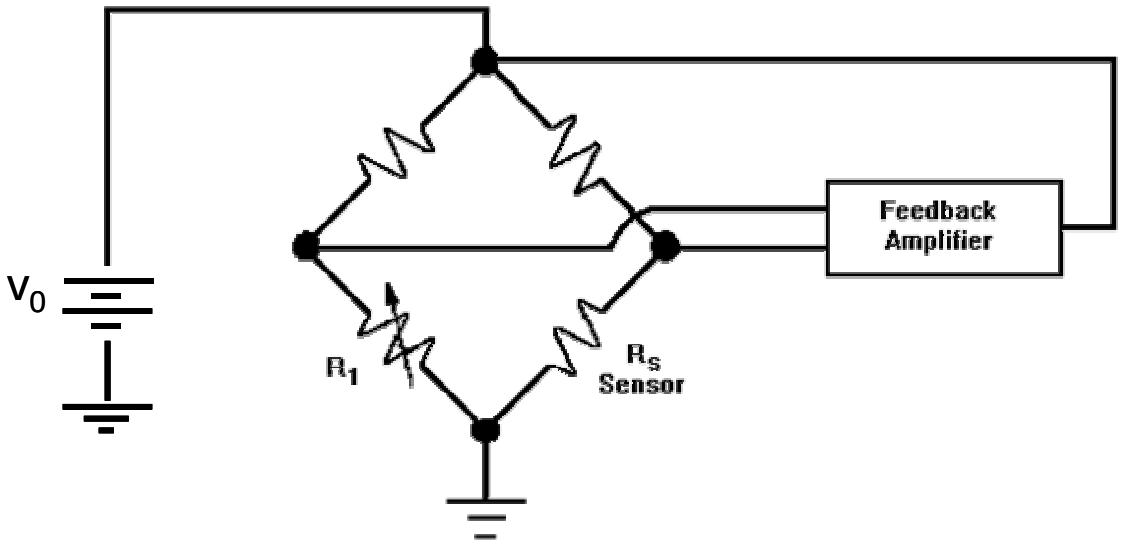

Figure 2-4 - Basic Wheatstone bridge circuit of the hot film anemometer

When the bridge circuit is activated, the applied voltage, called the bridge voltage, is imposed on the top node. As a result, a current flows down both legs of the bridge. If the resistance R_1 is higher than the sensor resistance R_s, the voltage input into the D-C differential amplifier will be non zero. The amplifier communicates this to the power supply and regulates the bridge voltage until the current passing through the sensor heats it to the exact temperature, and hence resistance, needed to balance the bridge. These adjustments happen very fast, usually on the order of a few microseconds. When a fluid having a temperature lower than the sensor flows over it, the bridge voltage fluctuates to regulate the sensor temperature until it is again constant. The ambient temperature, T_a and the sensor temperature $T_{s,}$ is related to the sensor resistance by Eq. (2.2.9), where α denotes the temperature coefficient of resistance (specific to each sensor).

$$R_s/R_a = 1 + \alpha(T_s - T_a) \tag{2.2.9}$$

The power dissipated in the heated hot film sensor is given by Eq. (2.2.10).

$$P = I^2R_s \tag{2.2.10}$$

Thus, the turbulent intensity, corresponding to the axial orientation of the hotwire probe, can be calculated by Eq. (2.2.11), where the numerator is the RMS (Root Mean Square) value of the velocity fluctuation u', and the denominator is the mean velocity as measured with the anemometer.

$$I_x \equiv \frac{\left(\overline{u_1 u_1}\right)^{1/2}}{U_o} \tag{2.2.11}$$

The electrical resistance of the sensor, R_s, can be approximated using a calibration curve that demonstrates a monotonically increasing voltage with flow. These curves are generated from the fundamental measurements of bridge voltage and velocity. Figure 2.5, below, shows a typical calibration curve where the bridge voltage is plotted against mass flux (lb/ft^2 -s).

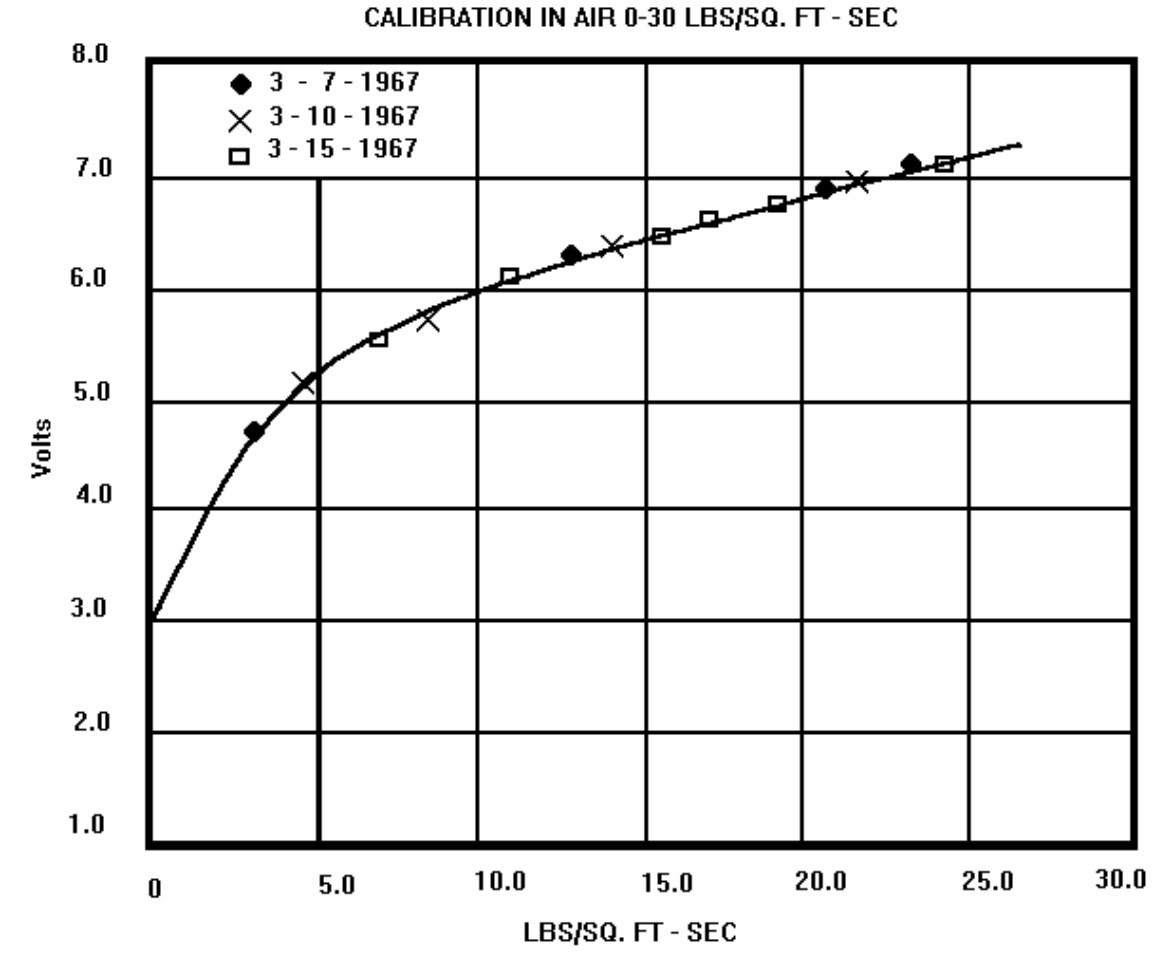

Figure 2-5 - Typical calibration curve, bridge voltage vs. mass flux

Turbulent intensity is determined from a calibration curve, similar to Fig. 2.5, which relates bridge voltage e_b to velocity. From the calibration curve, one would observe that

small fluctuations in flow velocity result in small changes in bridge voltage. Thus, turbulent intensity is usually a small number on the order of a few percent, and the slope of the calibration curve varies very little at operating points where the mean or time average velocity is constant. As such, fluctuations in the instantaneous bridge voltage are related to changes in flow velocity by Eq. (2.2.12), where B denotes the slope of the calibration curve.

$$e_b' = \mathrm{B}u' \tag{2.2.12}$$

Thus, the bridge voltage fluctuations can be related to turbulent intensity by Eq. (2.2.13) below.

$$I \equiv \frac{\left(\frac{\sqrt{e_b'^2}}{\mathrm{B}} \right)}{U_o} \tag{2.2.13}$$

The numerator is the RMS value of the bridge voltage divided by the slope of the calibration curve at the operating point, and the denominator is the measured steady mean velocity. Thus by Panton (1996), the overall turbulent intensity is defined by Eq. (2.2.14) as the average of the three respective axial turbulent intensities, I_x, I_y, and I_z corresponding to probe orientation.

$$I \equiv \frac{\left(\frac{1}{3} \overline{u_i u_i} \right)^{1/2}}{U_o} \tag{2.2.14}$$

For isotropic turbulence:

$$\overline{u_1 u_1} = \overline{u_2 u_2} = \overline{u_3 u_3} \tag{2.2.15}$$

and the turbulence intensity is equal to the axial component turbulent intensities.

$$I_x = I_y = I_z \equiv I \tag{2.2.16}$$

Thus, the data obtained through hotwire anemometry for the three probed Cartesian coordinate axes in the flow can be used implicitly to determine regions of isotropy.

Chapter 3. Wave Propagation through Random Media

3.1 Characteristics of Wave Behavior

Sound propagation through random media is the central part of this investigation. This chapter presents a frame of reference from which to understand the underlying acoustic principles of sound waves as they pertain to the measurements reported herein.

Any assembly of particles which mutually interact is a medium in which wave motion may occur. A brief disturbance in a small region induces motion in neighboring regions, resulting in some sort of movement which eventually spreads throughout the medium. This transmission of disturbances may be called wave propagation (Baldock, 1981). Consider a scalar physical quantity *u* which is dependent on a single space coordinate *x* and on a given time *t*. If, in some domain of *xt*-space, *u* can be expressed as:

$$u(x,t) = f(x - ct) \tag{3.1.1}$$

where *c* is constant,

then *u* is said to be a wave which propagates in an *x*-direction with velocity *c* (Baldock, 1981). Thus, every wave traveling with speed *c* in any *x*-direction satisfies the one-dimensional classical wave equation:

$$c^2 \frac{\partial^2 u}{\partial x^2} = \frac{\partial^2 u}{\partial t^2} \tag{3.1.2}$$

Likewise, a function $u(r, t)$ defined on a region of three dimensional space over some time interval is a plane wave moving in the positive x-direction by equation (3.1.1). On any plane perpendicular to the x-axis, u is constant, and the plane moves in a positive direction with constant velocity c. Hence, we can define this plane as the wave front. A plane wave moving in the direction of a unit vector n is defined by:

$$u = f(r \cdot n - ct) \tag{3.1.3}$$

From equation (3.1.3) we can derive the three-dimensional classical wave equation defined as:

$$c^2 \nabla^2 u = \partial^2 u / \partial t^2 \tag{3.1.4}$$

satisfied by all plane waves traveling with the same speed c (Baldock, 1981).

As outlined by Tatarskii (1961) in his discussion of sound wave scattering in a locally isotropic turbulent flow, the movement of sound waves through a turbulent flow stream is analogous to the phenomenon of electromagnetic wave scattering. The overall velocity of a propagating wave is influenced by the relative fluid velocity and surrounding temperatures. Temperature fluctuations are important as they cause fluctuations in the sound speed. The speed of sound can be expressed as:

$$c^2 = \gamma p / \rho = \gamma R T \tag{3.1.5}$$

for perfect gases,

$$\gamma = (R + c_v) / c_v \tag{3.1.6}$$

As shown by Eq. (3.1.5) above, the square of the sound speed is proportional to gamma, γ which ranges from a maximum of $5/8$ for monatomic gases through $7/5$ for diatomic gases, R the relative gas constant, and T the temperature.

Tatarskii (1961) gives the basic equation for sound propagation in a moving random medium to be written in the form:

$$\Delta P - \frac{1}{c^2}\left(\frac{\partial}{\partial t} + u_i \frac{\partial}{\partial x_i}\right)^2 P = 0 \qquad (3.1.7)$$

where P denotes the sound wave potential, u_i the components of the velocity motion of the described medium, and *c* the relative sound speed. More specific to our investigation, Andreeva (2003) outlines, at length, the applicability of two well known approximate theories of wave propagation, ray acoustics and the Rytov method.

3.2 Ray Theory and Statistics

Chernov (1960) described acoustic wave propagation in a medium with random inhomogeneities by ray theory and statistics. The theory is applicable provided that *a*, the scale of the inhomogeneities, is large compared to the wavelength λ. Thus, this condition is often satisfied for ultrasonic waves (Chernov, 1960). If this condition is satisfied, the application of ray theory is valid in regions of linear dimension *L*, where *L* satisfies the condition $\sqrt{\lambda L} << a$. However, at larger propagation distances the theory breaks down, and warrants the use of diffraction theory. Therefore assuming the following:

$$\lambda << a \tag{3.2.1}$$

$$\sqrt{\lambda L} << a \tag{3.2.2}$$

and that the transit time of the ray is small compared to the characteristic scale of changes of the inhomogeneities in time, the ray equation defined in Eq. (3.2.3) can be obtained from Fermat's principle.

$$\int_A^B \frac{d\sigma}{c} = \min \tag{3.2.3}$$

We can define the refractive index by:

$$n = \frac{c_0}{c} \tag{3.2.4}$$

Thus, Eq. (3.2.3) can be re-written in the form below:

$$\int_A^B n(x, y, z) d\sigma = \min \tag{3.2.5}$$

Furthermore, we assume that collectively, the ray trajectories are described by a family of curves expressed by the equations $x = x(u), y = (u)$, and $z = (u)$ that pass through given points A and B (Chernov, 1060).

The time taken for a ray to travel a given distance changes with varying conditions in the medium. This results in ray tube deformation, and subsequently intensity fluctuations (Chernov, 1960). Assuming that deviation of the rays from their

initial direction with respect of the x-axis is small, the travel time and mean travel time of a propagating wave over a distance L is given by:

$$t = \frac{1}{c_0}\int_0^L n(x,y,z)dx \tag{3.2.6}$$

$$\bar{t} = \frac{1}{c_0}\int_0^L \overline{n(x,y,z)}dx = \frac{1}{c_0}\int_0^L dx \tag{3.2.7}$$

where the corresponding values of the refractive index $n(x,y,z)$ are taken along the ray. Since $\bar{n} = 1$, the deviation from the mean time can be expressed by Eq. (3.2.8) as follows (Chernov, 1960).

$$\Delta t = t - \bar{t} = \frac{1}{c_0}\int_0^L n(x,y,z)dx - \frac{1}{c_0}\int_0^L dx = \frac{1}{c_0}\int_0^L \mu(x,y,z)dx \tag{3.2.8}$$

By assuming that the values of x in the correlation coefficient $N(x,y,z)$ are of the order $a(x \sim a)$, hence the mean square transit time fluctuations are defined by Eq. (3.2.9) (Chernov, 1960).

$$\overline{\Delta t^2} = \frac{2\overline{\mu^2}L}{c_0^{\,2}}\int N(x,0,0)dx \tag{3.2.9}$$

Thus, we can calculate the phase fluctuations $S' = \omega\Delta t$ by Eq. (3.2.10), and subsequently the relative change in intensity along a path dx by Eq. (3.2.11) below:

$$\overline{S'^2} = 2\overline{\mu^2}k^2 L\int_0^\infty N(x,0,0)dx \tag{3.2.10}$$

$$\frac{dI}{I} = -dx\int \nabla^2 \mu dx' \tag{3.2.11}$$

where *k* is the wavenumber (Chernov, 1960).

Subsequently these methods, based in ray theory, are generally used to describe the propagation of sound in a slowly changing medium state (Andreeva, 2003). The grid-generated turbulence in our experiment, to a large degree, is comparable to the turbulent atmosphere, featuring fluctuations in flow velocity and temperature. Equations (3.2.1) and (3.2.2) were used to determine if the conditions of the ray approximation is satisfied with respect to our investigation. The wavelength was determined by $\lambda = \frac{v}{f}$, where *v* is the propagation speed and *f* the respective frequency. Thus, for our 100 kHz transducers the wavelength was estimated to be approximately 3mm. The turbulent length scales as outlined in section 2.1 are not appreciably larger than the wavelength, and the left side of equation (3.2.2) as required. As such, the effect of these flow fluctuations on sound propagation cannot be treated by the methods of ray acoustics (Andreeva, 2003). Rather, a combination of the statistical representation of isotropic and homogenous turbulence and the Kolmogorov (1941) "2/3" law provide a foundation for the theory of wave propagation in turbulent media.

3.3 Kolmogorov's "2/3" Law and Resulting Travel Time Equations

Kolmogorov's "2/3" law states that the velocity fluctuations at two different points in the flow stream are proportional to the distance between these points raised to the 2/3 power (Frisch, 1995). Sound wave propagation between two transducers over a distance L, in a direction t_1 and opposite direction t_2, can be described by a derivation of the flowmeter equation (Andreeva, 2003). Accordingly, by Andreeva (2003) we can express the acoustic travel times of these waves as:

$$t_1 = \int_0^L \frac{dy}{c - u_1} \approx t_0 + \frac{1}{c^2}\int_0^L u_1 dy \tag{3.3.1}$$

$$t_1 = \int_0^L \frac{dy}{c + u_2} \approx t_0 - \frac{1}{c^2}\int_0^L u_2 dy \tag{3.3.2}$$

where t_0 denotes the travel time in the undisturbed media, and c the sound speed. The velocities u_1 and u_2 are defined by:

$$u_1 = U \sin\beta + u_1' \tag{3.3.3}$$

$$u_2 = U \sin\beta + u_2' \tag{3.3.4}$$

where U is the mean flow velocity, and u_1' u_2' are the respective fluctuations along the sound path. Neglecting terms of order U / c, U^2 / c^2, the time difference is expressed by Eq. (3.3.5) as follows:

$$\Delta t = t_2 + t_1 - 2t_0 \approx \frac{1}{c^2}\int_o^L (u_1' - u_2')dy = \frac{1}{c^2}\int_0^L \Delta u dy \tag{3.3.5}$$

The turbulent velocity fluctuations in Eq. (3.3.5) which influence the acoustic travel time can be described by a random function of time and position. Thus, Eq. (3.3.5) is rewritten as:

$$\overline{\Delta t^2} = \frac{1}{c^4}\int_0^L dy' \int_0^L dy'' \overline{\Delta u(y')\Delta u(y'')} \tag{3.3.6}$$

Invoking the Kolmogorov "2/3" law, we account for the correlation of fluctuations at different points in the flow, and so (Andreeva, 2003):

$$\overline{[u(y') - u(y'')]^2} = C^2 R^{2/3} \tag{3.3.7}$$

where R is defined by the distance between the points y' and y'', and C a constant characteristic of turbulence having dimensions of $cm^{2/3} \cdot s^{-1}$. Under the isotropic and homogenous turbulent assumption, the left hand side of Eq. (3.3.7) is expressed by Eq. (3.3.8).

$$C^2 R^{2/3} = \overline{[u(y') - u(y'')]^2} = 2\overline{\left[(u(y'))^2 - u(y')u(y'')\right]} \tag{3.3.8}$$

Thus, from transducer geometry we can define:

$$R_1^{\,2} = \delta^2 + (y' - y'')^2 \tag{3.3.9}$$

$$R_2^{\,2} = (y'' - y')^2 \tag{3.3.10}$$

By way of Eq. (3.3.9) and Eq. (3.3.10) and use of the "2/3" law, we rewrite the integrand of Eq. (3.3.6) as follows:

$$\overline{\Delta u(y')\Delta u(y'')} = C^2\left\{R_1^{2/3} - R_2^{2/3}\right\} = -0.5C^2\left\{2(y'-y'')^{2/3} - 2\left((y'-y'')^2+\delta^2\right)^{1/3}\right\} \quad (3.3.11)$$

Substituting Eq. (3.3.11) into Eq. (3.3.6) we define the expression:

$$\overline{\Delta t^2} = C^2 L\left(\frac{1}{c^2}\right)^2 \delta^{5/3} const \quad (3.3.12)$$

where the constant is determined experimentally by Obukhov (1951) to be equal to 3 (Andreeva, 2003).

3.4 Fermat's Principle

Fermat's principle states that the path of a ray of light between two points is the path that minimizes the travel time (for which it is an *extremum*). For example, let the ray traveling from a source in medium v_1 located at (0, a) to a receiver in medium v_2 at (b, -c), pass through the interface between the two media at some point (x, 0). To completely determine the ray path, we must find *x* such that the total travel-time T(x) for the path defined by *x* is an extremum.

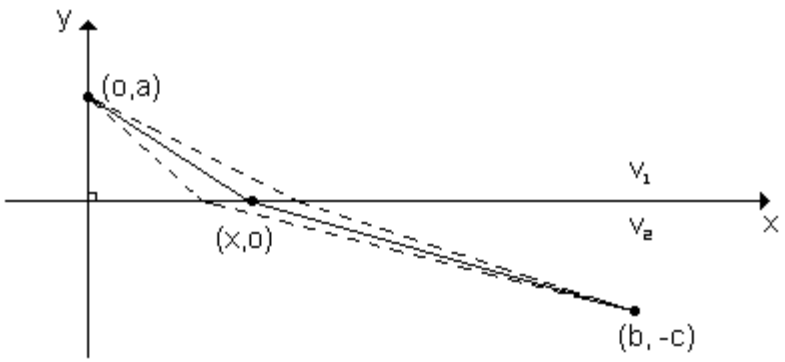

Figure 3-1 - Ray geometry defining minimum travel path

The time necessary for the ray to travel from (0, a) to (b, -c) via (x, 0) is defined by:

$$T(x) = \frac{\left(a^2 + x^2\right)^{\frac{1}{2}}}{v_1} + \frac{\left[(b-x)^2 + c^2\right]^{\frac{1}{2}}}{v_2} \tag{3.4.1}$$

Thus, to define *x* such that T(x) is an extremum, we set the first derivative to zero:

$$0 = \frac{dT(x)}{dx} = \frac{x}{v_1\left(a^2 + x^2\right)^{\frac{1}{2}}} - \frac{b-x}{v_2\left[(b-x)^2 + c^2\right]^{\frac{1}{2}}} = \frac{\sin i_1}{v_1} - \frac{\sin i_2}{v_2} \tag{3.4.2}$$

Hence, we arrive at Snell's Law:

$$\frac{\sin i_1}{v_1} = \frac{\sin i_2}{v_2} \tag{3.4.3}$$

Thus, so that the refracted ray path is actually a *minimum* time path we note that:

$$\frac{d^2T(x)}{dx^2} = \frac{a^2}{v_1\left(a^2 + x^2\right)^{\frac{1}{2}}} + \frac{c^2}{v_2\left[(b-x)^2 + c^2\right]^{\frac{1}{2}}} > 0 \qquad (3.4.4)$$

This relationship is also true for sound waves propagating between two different medium. With regard to our experiment, the principle states that the travel path between the ultrasonic transmitter and receiver always is an extremum. Hence, the length of the travel path, measured along a ray, is always shorter then any other path (Andreeva, 2003).

3.5 Caustics

The basic equations and methods of ray theory which describe wave motion throughout random media may become invalid as rays come within close proximity to each other to form caustics. The singularities of geometrical optics are caustics, and their systematization by catastrophe theory is perhaps the most significant application of that theory to date (Nye, 1999). The diffraction patterns associated with the caustics are dominated by wave dislocations, which are line singularities of the phase, analogous to crystal dislocations. A polarized wave field possesses an even finer structure of singularities (Nye, 1999). According to Lighthill (1978), a caustic is defined as a boundary between a region with a complicated wave pattern, due to interference between *two* groups of waves. In terms of ray theory, by Spetzler and Snieder (2001), the concept of caustics is understood as the focus point in space through which rays go; whereas the

consequence of their production in a wavefield is that the amplitude is infinitely high at the focus point because the geometrical spreading factor is zero at the caustic point.

The caustic phenomenon has been the focus of several investigations, such as those conducted by White et al. (1988), where he used limit theorems for stochastic differential equations on the equation of dynamic ray tracing to predict when caustics start to develop in Gaussian random media (Spetzler, 2001; Snieder, 2001). In addition, Kravtsov (1988) gave a thorough description of caustics, and Brown & Tappert (1986) used Chapman's method to write explicitly the variation of 2-D and 3-D wavefields in the vicinity of focus points (Spetzler, 2001; Snieder, 2001). Lighthill (1978) uses the Airy integral to address the contradictions of a straightforward ray acoustics theory and account for the local singularities in the presence of the caustics. However, for our purposes we will narrow the scope of our interest to the behavior of propagating waves before they strongly interact to form caustics, but, interact strongly enough for their influence to be seen in the non-linearity of the amplitude variance.

Chapter 4. Experimental Apparatus

All experiments were performed inside a rectangular test section of normally low turbulence, in a low speed open circuit type wind tunnel. The generated isotropic turbulence was realized by way of a stationary grid fixture positioned upstream of the test section. The ultrasonic travel time technique was used to diagnose the turbulent flow parameters utilized in our investigation. The experiment was designed to ensure that the region of non-linearity in the acoustic travel time variance with respect to the travel distance and occurrence of the caustics would be realized. The latter sections of this chapter describe the essential elements of the experimental apparatus including: the wind tunnel, grid fixture and geometry, ultrasonic measurement systems, temperature monitoring controls, and the data acquisition and analysis system.

4.1 Wind Tunnel

The AEROLAB low speed, low turbulence wind tunnel used to provide and maintain the turbulent flow conditions is an Eiffel or Open Circuit type, with a rectangular test section measuring 45.25” in length, 11.75” wide and 11.62” high. Airspeeds of 0 to 80 mph were produced by an infinitely variable control system, enabling smooth transitional increases over the entire range. Aerodynamic losses and mean flow instability were minimal due to the tunnel’s high energy ratio, achieved in part through a contraction ratio of 16:1, a small angle diffuser and an efficient fan system.

The AEROLAB wind tunnel consists of three main sections: the fan unit, the test section, and the diffuser as shown in Fig. 4.1.

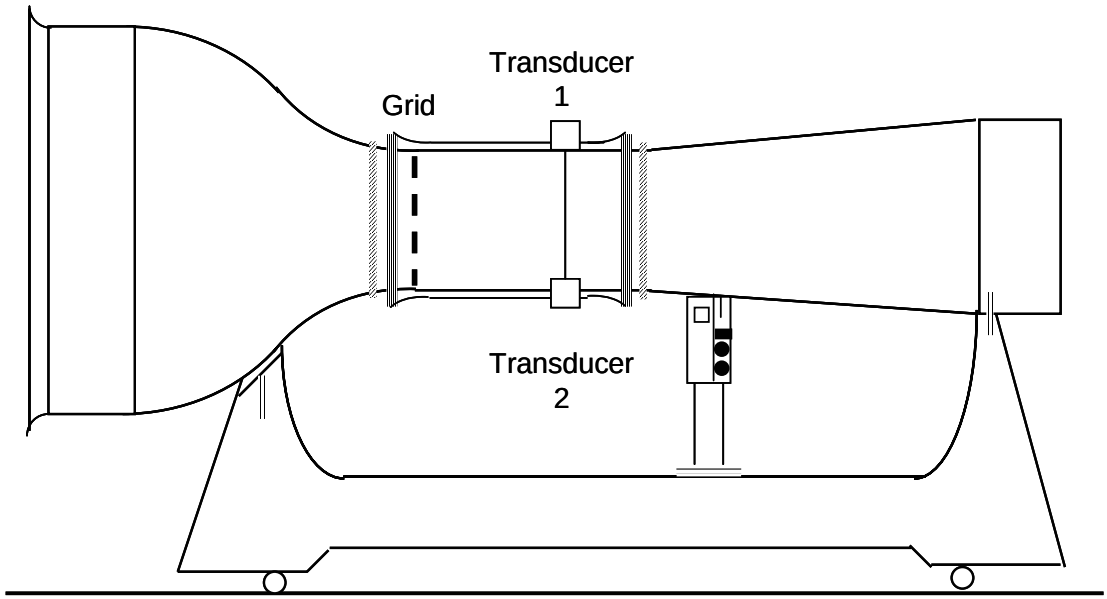

Figure 4-1 - AEROLAB wind tunnel

A passive noise reduction system, in the form of an acoustic damping blanket, line the inside cavities of the fan section to reduce unwanted vibrations and noise. The tunnel's test section was entirely rebuilt and retro fitted with Lexan plates designed specifically to operate in concert with other experimental systems. GE Lexan was chosen over traditional fiberglass (which the previous test section was constructed from) due to its ease in machining. High density polyvinyl rubber foam was applied to the perimeter of the access panel sealing surfaces to increase the integrity of the seal and minimize pressure losses. The interior panels were also sealed, using quick dry putty that was worked into the smaller areas of the test section.

Lastly the diffuser was equipped with an aluminum honeycomb, four turbulence management screens, and orifice rings both in the contraction and upstream used to

compute the airspeed from the differential pressure drop across both ends using an external digital manometer with integrated pressure transducer. The digital readout enabled monitoring of the differential pressure in inches of water with a high level of accuracy. Thus, flow speed was determined by inputting these pressures in inches of water into a modified Bernoulli's equation as defined by Eq. (4.1.1) - (4.1.3):

$$P_T = P_S + \frac{1}{2}\rho V^2 \tag{4.1.1}$$

$$\Delta P = \frac{1}{2}\rho V^2 \tag{4.1.2}$$

$$\sqrt{\frac{2\Delta P}{\rho}} = V \tag{4.1.3}$$

where P_T and P_S are the total and static pressures respectively, ρ the air density and V the flow speed.

Air flowing into a test section forms a boundary layer on the walls of the tunnel. It is determined that for this flow the boundary layer displacement thickness is given by:

$$\delta^* \sim 0.0033x^{\frac{1}{2}} \tag{4.1.4}$$

where x is a distance downstream of the grid-fixture in the tunnel (Andreeva, 2003). Thus, it can be estimated that the maximum displacement thickness $\delta^* \sim 0.0027m$ corresponding to the measurements taken at x = 0.68m downstream of the grid. Thus, boundary layer interacts were avoided during experiments by maintaining a minimum of approximately 1 ¼ inch clearance from the walls of the test section.

4.2 Grid-Fixture & Resulting Turbulence

The generated turbulent flow was the result of a stainless steel welded wire mesh grid fixture situated upstream of the flow at the entrance of the test section. The fixture consisted of two square frames that when clamped together served as a mounting platform for the two different square welded wire meshes screens that were used in the experiment. The upper and lower sections of the framing were machined down to a minimum thickness in order to minimize the perturbation to the near wall flow (i.e. production of turbulent eddies after the grid threshold) by the introduction of a step in the flow stream. A consistent origin of turbulent flow generation was maintained by positioning the fixture behind two set-screws in the wind tunnel.

Grid-turbulence is made by disrupting laminar flow with a grid to generate a set of jets. These jets will interact with the air at rest behind the bars, become instable and make the transition to turbulence. The mesh size, or distance between centers of the stainless steel mesh rods, is one of the critical parameters that are used to determine the resulting turbulent flow. In our investigation two different mesh sizes of 0.25" and 0.50" were used. The two different grid mesh sizes were chosen based on there relationship to the plot of the acoustic travel time variance, with the x-axis proportional to the ratio of the characteristic length to the grid mesh size as shown in Fig. 1.2. Graphically, varying these grid mesh sizes along with the flow velocity allowed use to populate the upper regions of Fig. 1.2 that correspond to larger length scales.

4.3 Ultrasonic Measurement System

The ultrasonic measurement system consisted of two subassemblies supporting the ultrasonic transducers to form the flow diagnostics apparatus. The transducers produced and sensed ultrasonic waves. Transducers, by definition, are any mechanism or device that converts input energy of one form into output energy of another. The transducers in this study were a low frequency narrow band disc type of 100 kHz working frequency, operated with a high degree of precision based on the underlying material characteristics of asymmetrical crystals and the piezoelectric effect.

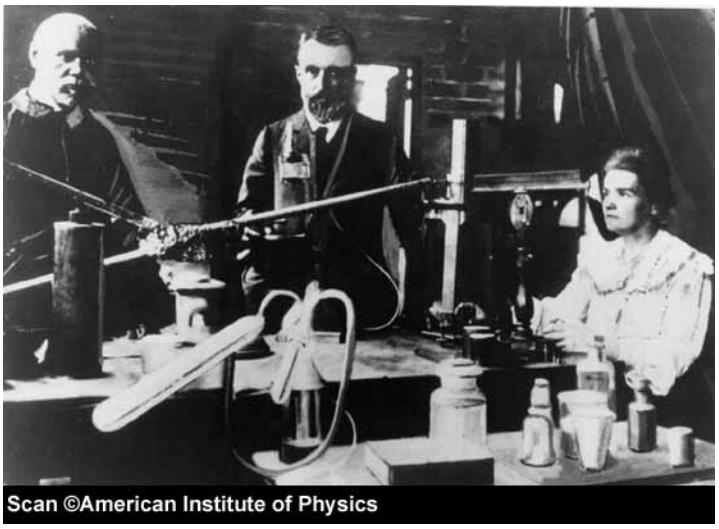

Figure 4-2 - Pierre Curie (center), and Marie Curie (left) in their laboratory, awarded half of the Nobel Prize for Physics in 1903.

Historical references to the piezoelectric effect date back to 1880 and the Curie's who established that crystals which lack a centre of symmetry when compressed along a certain axes develop positive and negative charges of magnitude proportional to the applied pressure (Richardson, 1962). Conversely, they also observed changes in the

crystals dimensions when a potential difference was applied. From these observations it was determined that an oscillating potential when applied could deform the crystals at a high rate of change to produce mechanical vibrations. As such, piezoelectric transducers are designed to be used as both transmitters and receivers.

The monolithic piezoelectric plate transducer is an assembly of piezo-crystals and dynamic mechanical components with interspersed electrical circuitry. The main components can be characterized by the active element, backing, and wear plate. The active element is usually constructed from piezoelectric or ferroelectric material; although a combination of other materials as of late are becoming more common. It converts an oscillating electric potential, such as an excitation signal from a function generator, into ultrasonic sound waves. The backing is usually a damping material of high density, used to control the vibration of the transducer by absorbing the overflow of energy that radiates from the back face of the active element. The wear plate is a protective structure used to shield the transducer elements from their environment.

The Curie constant describes the relationship between crystalline deformation and excitation energy by the ratio of mechanical movement to the applied voltage. Various piezoelectric crystals can be used as oscillators such as tourmaline, Rochelle salt, and ammonium dihydrogen phosphate (ADP) in multiple configurations.

The nominal detection range of an ultrasonic distance is determined by the operating frequency in two ways. First, the attenuation coefficient α of ultrasound, which increases with the operating frequency, establishes a firm limit as to the *maximum* distance at which even good reflecting objects can be detected (Lynnworth, Mágori, 1999). Second, the decay time of the ultrasonic signal at the transducer after a

transmission is inversely proportional to the operating frequency, which in turn dictates a minimum distance at which objects can be observed. These factors are all both critical to the arrangement of the ultrasonic transducers within our experimental apparatus, and integral in exploiting their operational capabilities.

The remainder of the section describes the structural components of the ultrasonic apparatus and their functionally with respect to the larger system.

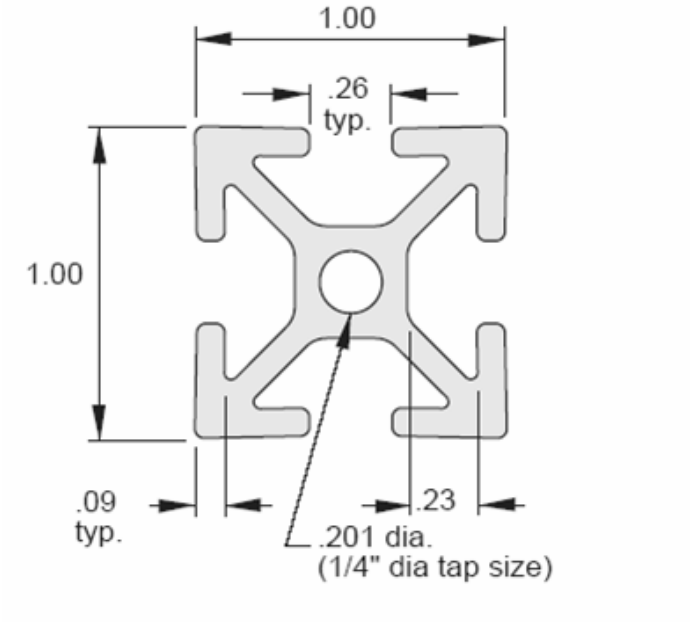

Figure 4-3 – 6105-T5 Aluminum Extrusion Cross Section

The primary transducer support structures were fabricated from 6105-T5 Aluminum EX-11 ¼" slotted extrusions and represent the skeleton of the ultrasonic flow meter. The slotted rectangular beams were fastened together using flanged button head cap screws and T-nuts in a rectangular frame configuration, bisected by a single rail. This interior railing represents the active site of the fixture on which a single mount linear bearing was placed to control the movement of the active member. The active member in our apparatus denotes the ultrasonic transducers responsible for transmitting and

receiving ultrasonic waves after they traverse the mean flow. Both transducers were partially submerged in the flow, and their movement controlled externally. In this configuration, the ultrasonic path lengths were varied by sliding the transducers, placed atop of the linear bearing mounts, along the center railing for angular orientations. For perpendicular orientations, the ultrasonic path lengths were varied by sliding the entire main structure up or down along the six stationary support beams affixed to the tunnel. Additionally, a set screw was placed on the side of the bearing mount to allow the linear bearings to operate from a stationary position on the railing during wind tunnel operation.

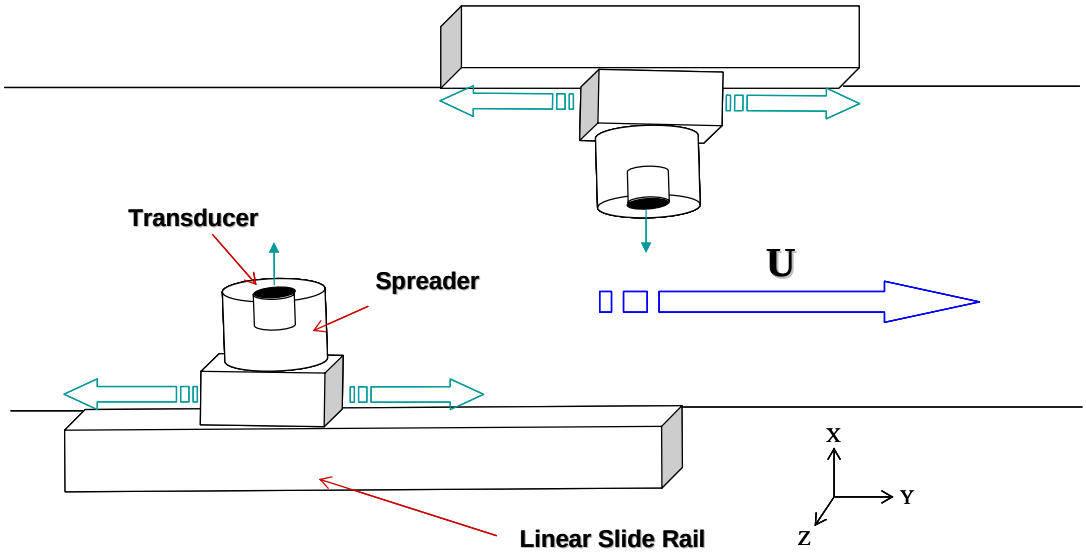

Figure 4-4 - Schematic of Linear Slide Rail Operation

To minimize flow interactions with the ultrasonic transducers that are present in the mean flow path, they were placed inside protective streamlined coverings made from sailboat spreaders. Sailboat spreaders are designed and used to decrease the overall drag on the rigging used to support masts of high performance sailboats. As such, we are using these structures for a similar purpose.

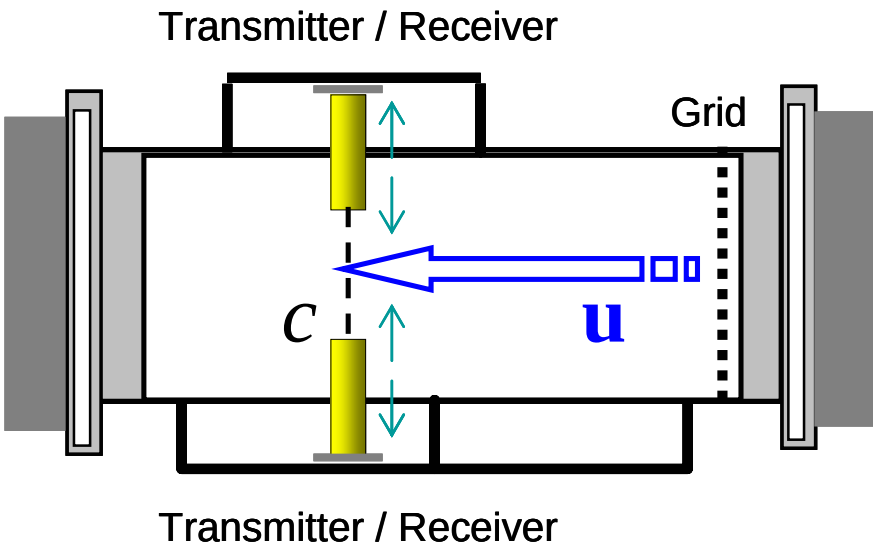

Figure 4-5 - Path length variation in perpendicular orientation

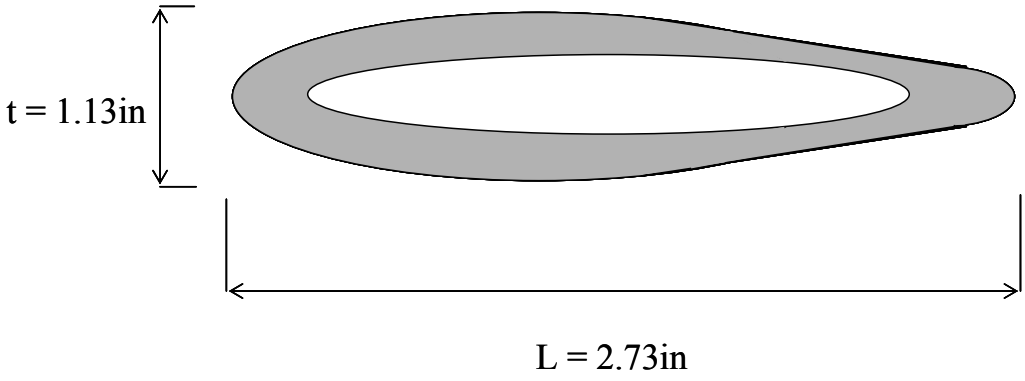

Figure 4-6 - Spreader cross-section

The spreaders reduce the overall wake produced by the ultrasonic transducers and related wiring, thus preserving our desired flow characteristics and minimizing vortex shedding from the transducer supports. The length of the two spreader

components (approximately 7.25” each) was dictated by the minimum ultrasonic propagation distance chosen for this investigation of approximately 1.97 inches.

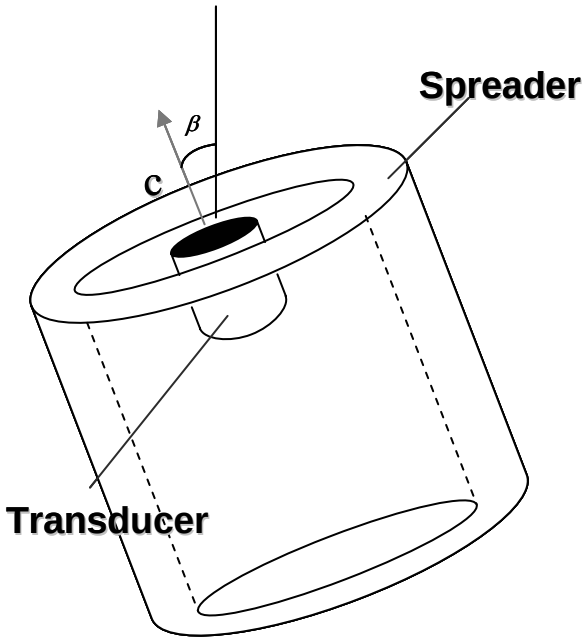

Figure 4-5 - Transducer Spreader Sub-Assembly

This minimum propagation distance was achieved by maintaining tight tolerances set for machining the spreaders in addition to fine adjustments made to the levels of the support structures affixed to the wind tunnel. All subsequent ultrasonic path lengths were increased as described previously. However, angular experimental orientations demanded that the spreaders be angled to preserve the line of sight between transmitter and receiver as they were moved further apart along the center railing. Transducer line of sight was verified using the Hewlett Packard 54645A/D Oscilloscope to visually observe the maximum amplitude of the received signal with respect to the spreaders angular

orientation. Angular mobility was achieved through custom T-brackets and pivot joints affixed to the top of the linear bearings.

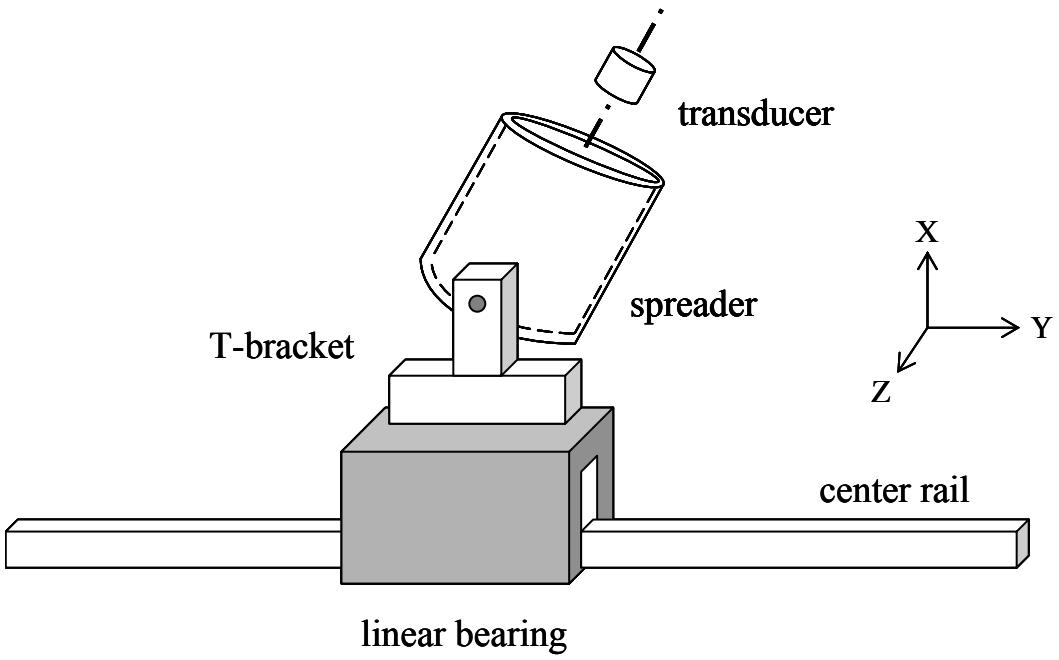

Figure 4-8 - Complete Spreader Assembly

The resulting fabricated apparatus as described represents the bulk of the mechanical fixtures present in our ultrasonic flow diagnostics apparatus. The remaining portions represent electrical components integral in the generation, processing, and overall computation of acoustic travel times as outlined in the subsequent explanation of our data acquisition systems.

4.4 Temperature Monitoring Controls

The temperature inside the wind tunnel test section was monitored effectively using an Omega DP41-TC high performance temperature indicator and fast thermocouple. The temperature indicator was configured for use with fast thermocouples and featured a cold junction board which applied the sustaining reference voltage from which to measure temperature changes. The digital temperature indicator and thermocouple combination was capable of monitoring temperature fluctuations in the mean flow of 0.2 degrees Celsius and 0.3 degrees Fahrenheit. The J type thermocouples used were rated to operate in temperatures from -210 to 760 C and -346 to 1400 ^{o}F. The J thermocouple was passed through a small hole in the top of the wind tunnel test section and placed in stream of the mean flow far downstream of the grid fixture. Monitoring the flow temperature during data acquisition allowed for rough estimates of the acoustic travel time to be made based on sound speed. Moreover, experiments were only conducted during periods of constant temperature within +/- 0.2 ^{o}F.

4.5 Data Acquisition System

The major components of the data acquisition system are shown in Figure 4-12. These primary components included the function generator, amplifier, oscilloscope, National Instruments data acquisition card, CompuScope data acquisition card, and the controlling PC.

4.5.1 Acquisition System Hardware

A Hewlett Packard 3314A programmable function generator was used to produce the excitation signal that controlled the composition of the transmitted waves. This function generator was triggered externally by the PC to initiate the ultrasonic pulses, thus enabling the data acquisition software to record the exact instance of each transmission. The generator was set to transmit bursts of four square waves at 100 kHz frequency with amplitudes of 50 mV. To boost the signal, it was passed through an Amplifier Research 50A15 power amplifier before it was sent to the transducers.

A Hewlett Packard 54645A/D Oscilloscope was connected directly to the function generator and receiving transducer to observe the transmitted and received signals and check for abnormalities. The oscilloscope featured 16 digital and 2 analog channels with a range of 1mV/div – 5V/div and maximum input of 400V. Ultimately this device served as a secondary confirmation of the excitation and received signals that were monitored primarily by the LabView National Instruments data acquisition software. The instrument was also used to measure the alignment (i.e. line of sight) of the ultrasonic transducers while conducting tests in the angular configuration. The orientation of the transducers was varied until the received signal was observed to have achieved maximum amplitude.

For acoustic time of flight measurements, the two most important pieces of information pertaining to each ultrasonic wave is the exact instance that the wave was initiated and then received after it traverses the mean flow. These two times were used to compute the acoustic travel time of the wave using a correlation function. A comparison

of the difference in transit time between the no-flow and turbulent flow situations allowed for an accurate determination of the mean flow's dynamic contribution to the traveling wave propagation. The departure times corresponding to the instant of transmission of the ultrasonic wave bursts are detected by the NI-DAQ with a high degree of accuracy. On each rise of the square wave pulse, the system is triggered and thus the departure time of the wave is recorded.

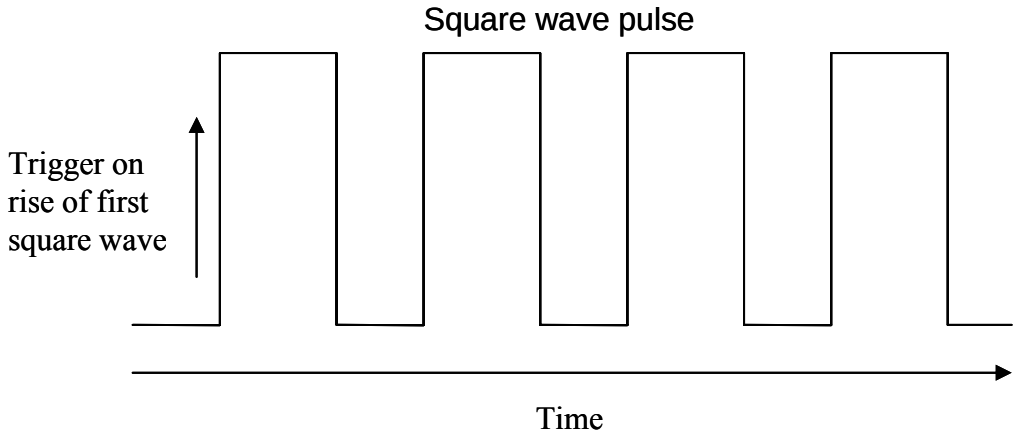

Figure 4-9 - Transmitted Square Wave Burst Signal

The two signals, sent and received, were correlated using LabView to determine the acoustic travel time. The programs correlation function was written as:

$$K_{12}(t) = \overline{e_1(t+\tau)e_2(t)} \tag{4.5.1}$$

The correlation function was written into a signal correlation program in IMSL Fortran programming language, as described in detail in Appendix B.

Each correlated sent and received signal yields a corresponding travel time. For example, Fig. 4.10 illustrates a typical sent and received signal acquired by the CompuScope 82G system.

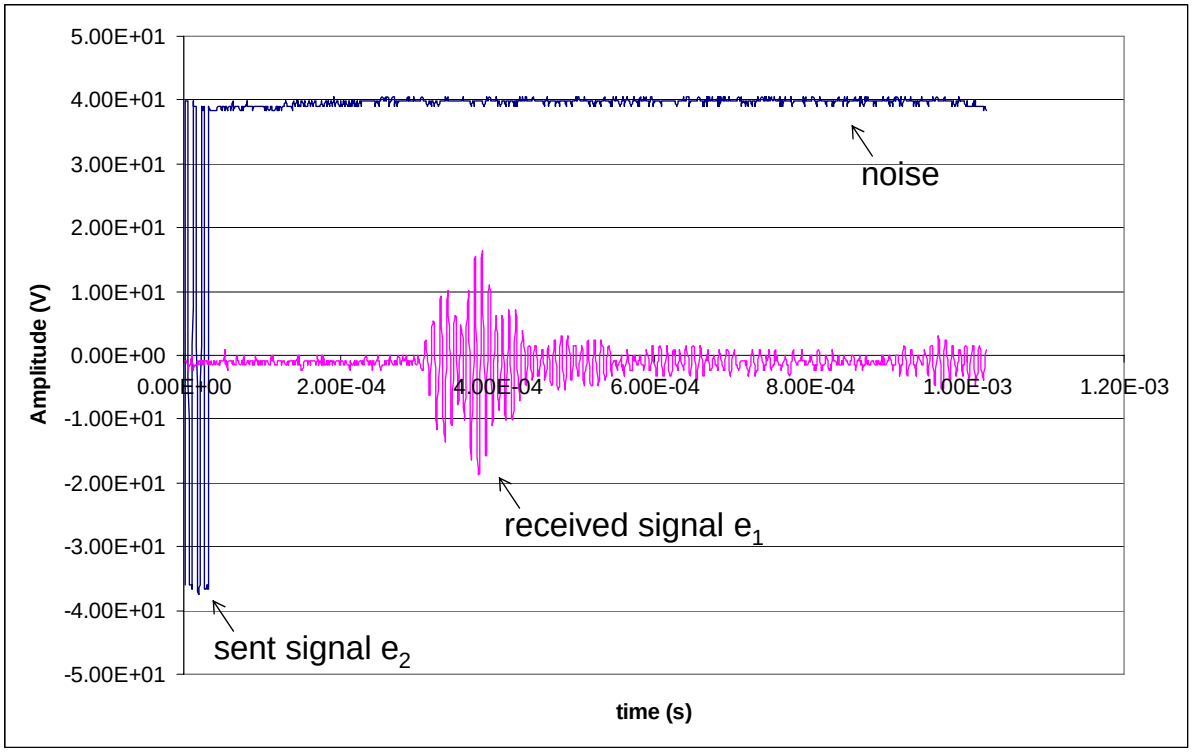

Figure 4-10 – Sent and received wave signals e_2 and e_1 respectively

These two signals are input into the IMSL Fortran signal correlation program, and its output, as illustrated in Fig. 4.11, is the correlated signal. Thus, the maximum amplitude of the correlated signal corresponds to the acoustic travel time of the transmitted wave.

Over a period of 45seconds with the NI-DAQ transmitting the square wave pulse at 500 cycles/sec, approximately 700 travels times were collected, and used to compute the travel time variance as follows:

$$\tau^2 = < (t_i - < t >)^2 > \qquad (4.5.2)$$

where the brackets surrounding each parameter indicate averaging over the data set.

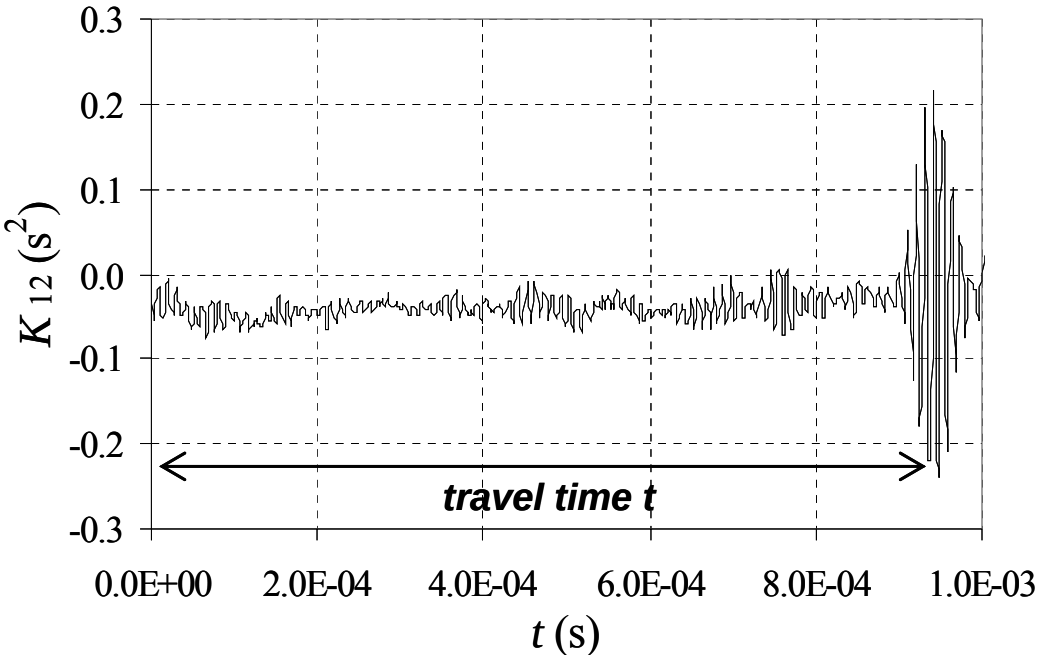

Figure 4-11 – Correlation of sent and received signals e_1 and e_2 taken from Andreeva and Durgin (2003)

The CompuScope 82G DAQ card was used to sample and store data corresponding to the two signals, sent and received, along with a sampling time marker for each wave. This data acquisition card featured 2 channels with monolithic A/D converters each running at 1 GS/s, 400 MHz band width, 8 bit resolution, and was designed to allow maximum separation of analog and digital grounds, thereby providing high immunity to digital noise. The card, manufactured by GaGe Applied Science Inc., is controlled through a LabView interface called Gage Sample Oscilloscope.vi which was

supplied with the board. From this module, the sampling rate, trigger type, number of data points collected, clock speed, sent and received signals, etc. were monitored and controlled. All acquired data was recorded and saved automatically by the system as a tab delimited text file for each test run.

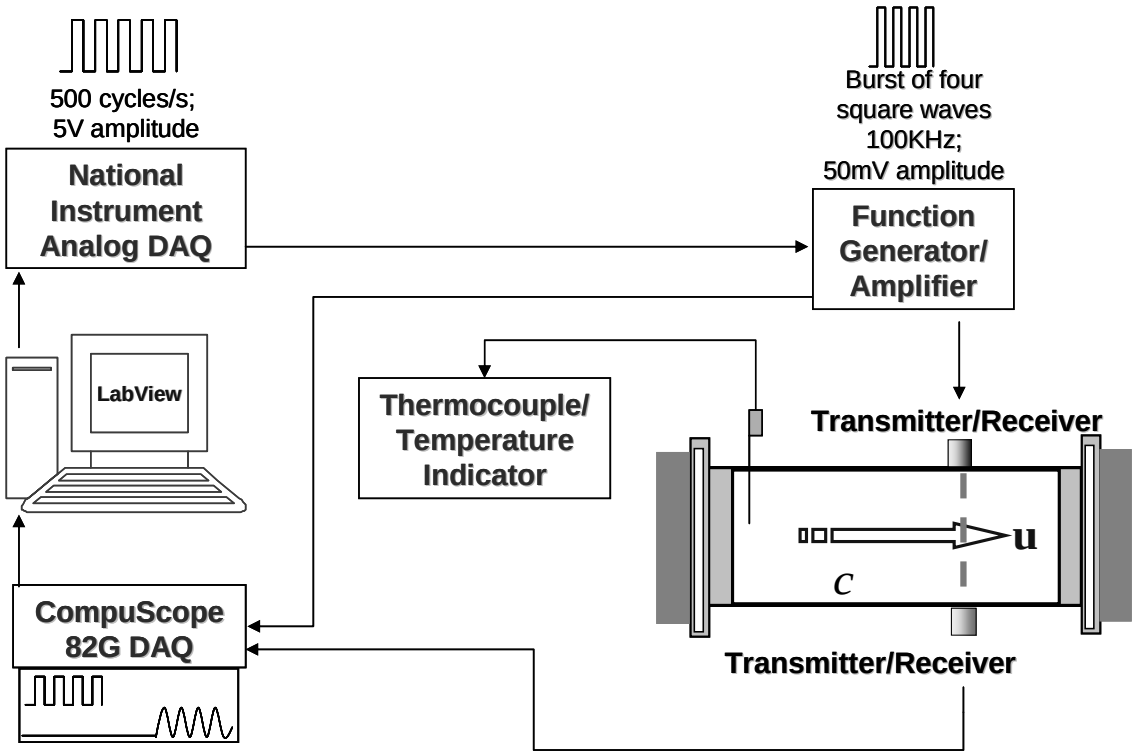

Figure 4-12 - Data Flow Diagram

Thus, Fig. 4.12 is a graphical representation which summarizes the flow of acquired data through hardware and system components. Likewise Fig. 4.13 illustrates all hardware interconnections.

The primary data analysis was conducted using LabView 5.1, and the following describes the details of the data acquisition software.

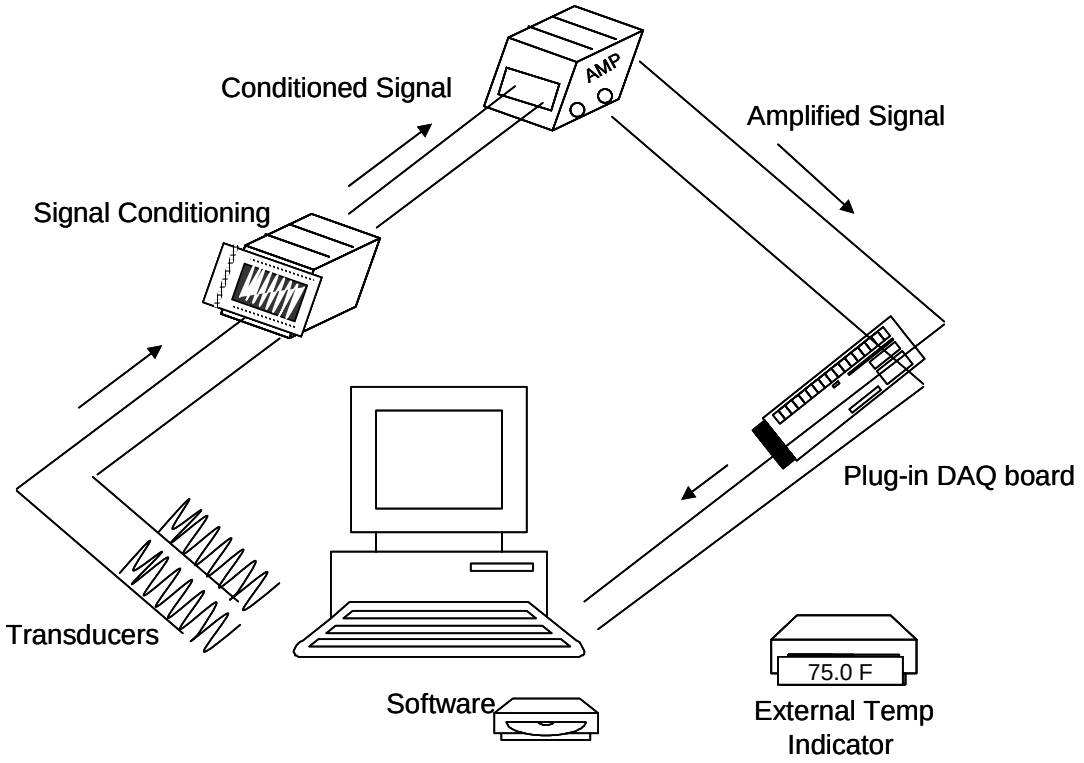

Figure 4-13 - Hardware Flow Diagram

4.5.2 Acquisition System Software

All of the hardware data acquisition systems were controlled using LabView 5.1 programs. The Function Generator.vi program was used to trigger the Hewlett Packard 3314A programmable function generator. This program, as illustrated in Fig. 4.14, enabled the exact instance that each ultrasonic wave was sent to be determined with a high degree of accuracy and precision.

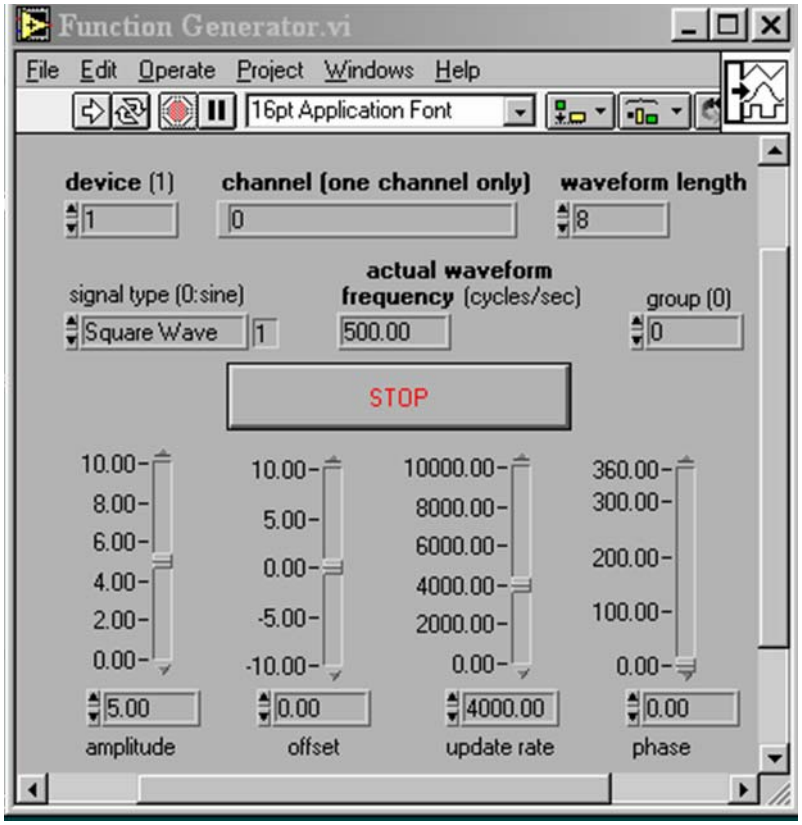

Figure 4-14 - Function Generator.vi

The Gage Sample.vi program was used to control the CompuScope 82G high speed data acquisition card. This program, as illustrated in Fig. 4.15, controlled the signal sampling rate and channel voltages.

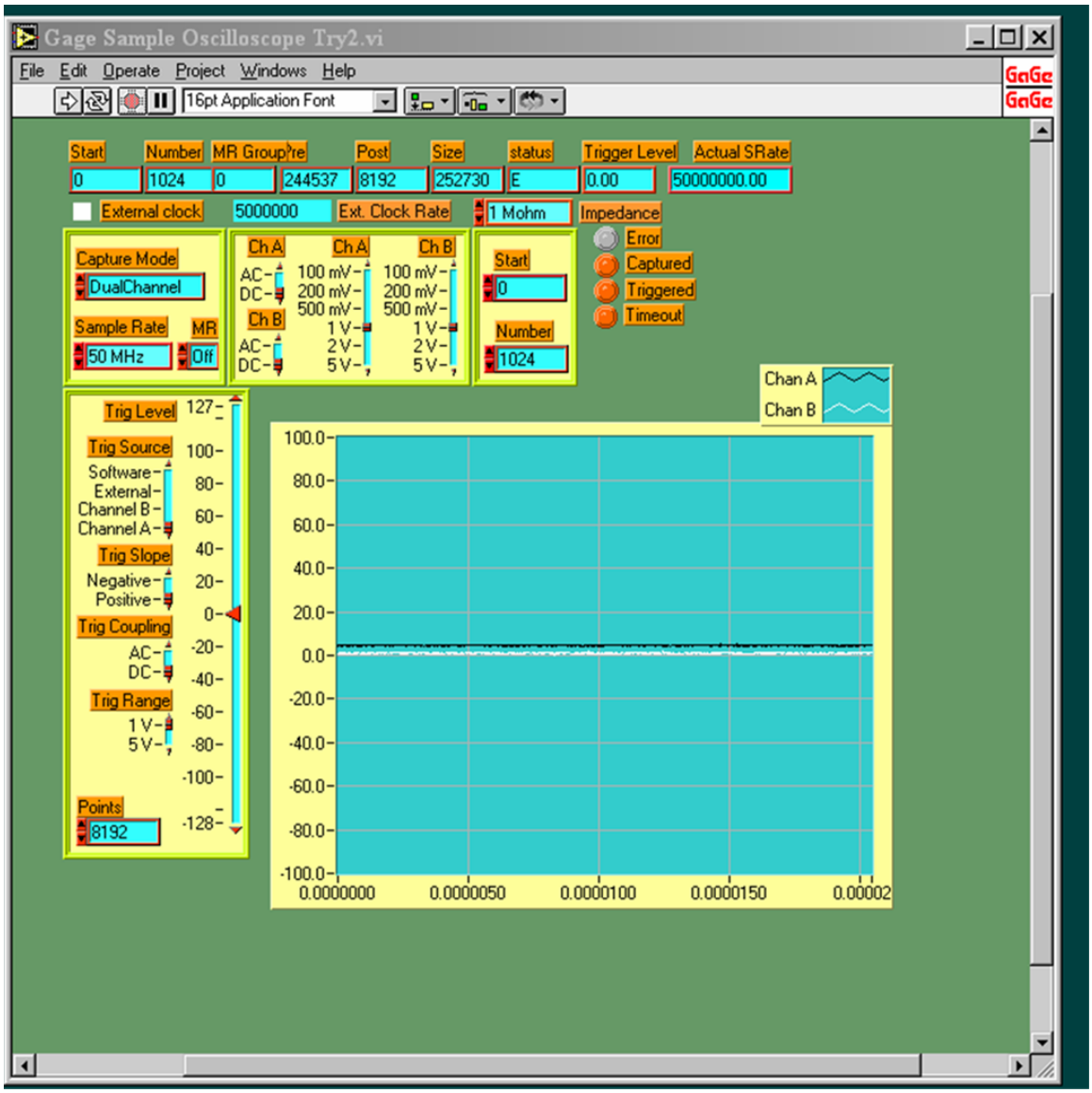

Figure 4-15 - Gage Sample.vi

An integral part of this program was a sub vi (virtual instrument) called CSScope.vi, developed by Gage to configure and initialize the data acquisition card. A detailed view of the CSScope.vi is presented in Appendix A.

Chapter 5. Experimental Results and Discussion

In this chapter we present the results and analysis of our experimental data, having applied the travel-time ultrasonic technique for data acquisition in a grid-generated turbulence.

5.1 Travel-time Ultrasonic Techniques for Data Acquisition

In the present study we consider a locally isotropic turbulent flow, generated by a welded wire mesh grid fixture placed in stream of a uniform flow, as done previously in studies by Batchelor and Townsend (1948), Mohamed and LaRue (1990), Comte-Bellot and Corrsin (1966), and Sreenivasan et al. (1980). At a considerable distance downstream of the grid, the flow becomes locally isotropic in nature, and thus the decay power law is applicable. Studies that quantitatively identify in detail this region downstream of the grid, that is considered to be nearly homogenous and locally isotropic, are those by Mohamed and LaRue (1990), Comte-Bellot and Corrsin (1971), and Uberoi and Wallis (1967). Thus, experimentally, regions downstream of our welded wire mesh grid fixture, as well as the respective mean flow velocities, were chosen based on the methods outlined by Mohamed and LaRue (1990). As a result, the 25” – 42” portion of the test section was used to collect our experimental data; with the bulk of the data presented within collected at 27” downstream of the grid.

As presented in Chapter 4, the transducers in our experimental apparatus worked as both transmitters and receivers depending on orientation. For each given experimental run, which corresponds to a different ultrasonic path length, more than 1000 travel times were used to compute each mean travel time. Additionally, data was collected for 45 seconds during 0.25in grid experiments, and for 30 seconds during 0.5in grid experiments. Thus, each tab delimited text file output by the CompuScope 82G data acquisition card was approximately 15 and 9 Megabytes, for 45 and 30 second runs respectively. The travel time for each ultrasonic pulse was determined using the cross-correlation function defined in Eq. (5.1.1) below:

$$K_{12}(t) = \overline{e_1(t+\tau)e_2(t)} \tag{5.1.1}$$

where e_1 and e_2 denote the received and transmitted waves, as illustrated in Fig. 4.7. Thus, by definition, and assuming the process to be ergodic:

$$K_{12}(t) = \frac{1}{T}\int_0^T e_1(t+\tau)e_2(t)dt \tag{5.1.2}$$

where the acoustic travel time t_n is determined by:

$$K_{12}(t) = K_{12}(t_n) \tag{5.1.3}$$

Thus, we consider N data values $\{x_n\}, n = 1,2,...,N$ sampled at equal time intervals dt from a transformed record $x(t) = x(ndt)$. As such, the cross-correlation function of $x(t)$ is estimated from the sample values at the time delay rdt by Eq. (5.1.4).

$$K_{12}(rdt) = \frac{1}{N-r}\sum_{n=1}^{N-r} x_n x_{n+r}, r = 0,1,2,...,m \qquad (5.1.4)$$

Approximately *Nm* real multiply-add operations are needed to compute the cross-correlation function of the received and transmitting signals. Taken from Andreeva (2003), the numerical code used to compute the cross-correlation functions of two stationary time series K_{12} was written in IMSL Fortran featuring a CCF module. A complete text version of the code is presented in Appendix B.

5.2 Travel-time Fluctuations based on Ultrasonic Path Length

The data presented in this section was collected for varying ultrasonic path lengths at 2, 3, 4, 5, 6, 6.5, 7, 7.5, 8, 8.5, 9, and 10 inch transducer separations. Figure 5.1 illustrates the upper and lower fixtures used to position the shielded transducers in and out stream of the flow path. Detailed photos of the ultrasonic supporting apparatus are presented in Appendix C. The experiment was performed for mean velocities of 0, 5, 10, 18, and 20 m/s. Figure 5.2 and Table 5.1 featured below; illustrate the 0.25in grid mean travel time data.

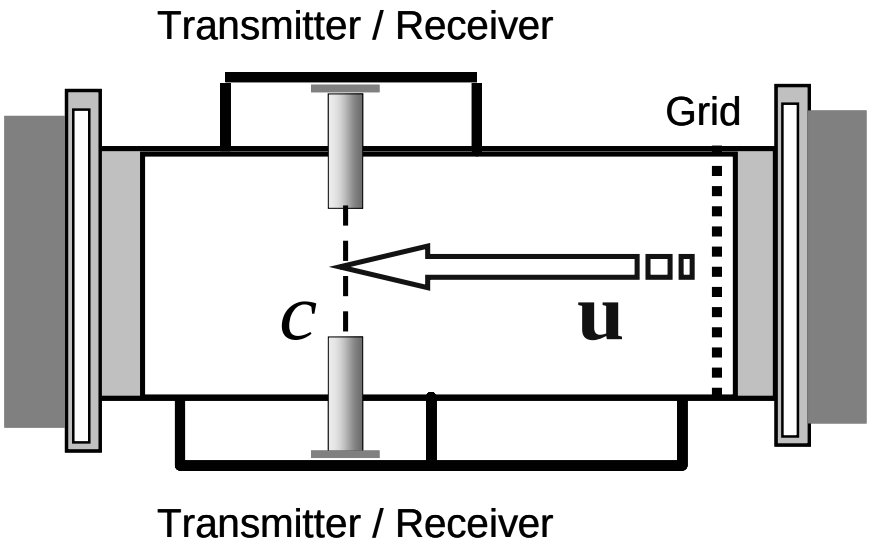

Figure 5-1 - Ultrasonic supporting apparatus mounted to wind tunnel test section

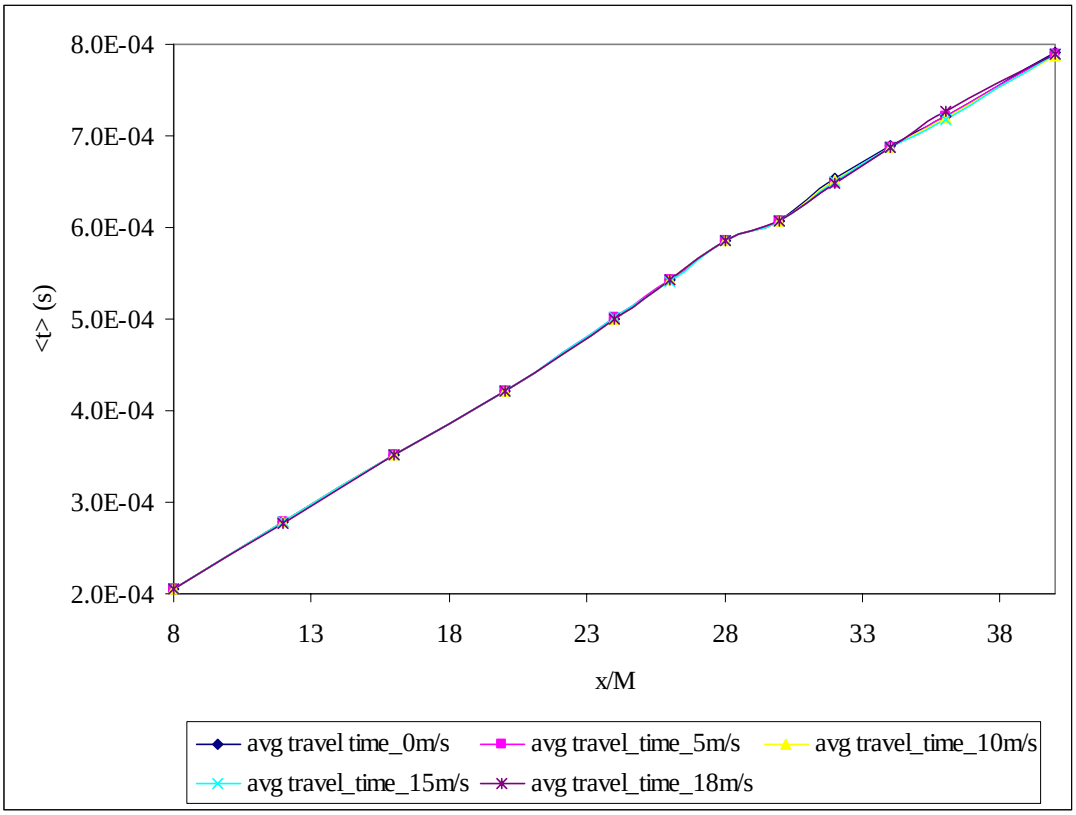

Figure 5-2 - Mean travel time vs. Non-dimensional length scale 0.25in grid

distance (x/M)	average travel time 0m/s	average travel time 5m/s	average travel time 10m/s	average travel time 15m/s	average travel time 18m/s
8	2.05776E-04	2.05678E-04	2.0538E-04	2.0484E-04	2.0474E-04
12	2.78918E-04	2.78774E-04	2.7828E-04	2.7800E-04	2.7732E-04
16	3.51961E-04	3.52008E-04	3.5180E-04	3.5196E-04	3.5108E-04
20	4.22003E-04	4.21947E-04	4.2164E-04	4.2200E-04	4.2130E-04
24	5.00890E-04	5.01142E-04	5.0026E-04	5.0098E-04	5.0012E-04
26	5.43496E-04	5.42880E-04	5.4261E-04	5.4175E-04	5.4252E-04
28	5.85415E-04	5.86003E-04	5.8568E-04	5.8520E-04	5.8559E-04
30	6.07333E-04	6.07383E-04	6.0636E-04	6.0714E-04	6.0688E-04
32	6.52782E-04	6.48692E-04	6.5147E-04	6.4916E-04	6.4849E-04
34	6.88493E-04	6.88192E-04	6.8837E-04	6.8779E-04	6.8815E-04
36	7.21771E-04	7.21723E-04	7.2017E-04	7.1865E-04	7.2681E-04
40	7.90842E-04	7.89104E-04	7.8837E-04	7.8931E-04	7.8904E-04

Table 5-1 - 0.25in grid mean travel time table

It can be seen from the positive slope of the data in Fig. 5.2 that the average travel times increase with increasing path lengths, as can be expected. However, apparently, the turbulence was not intense enough to illustrate Fermat's principle; which predicts a decrease in the acoustic travel times with increasing turbulent intensity. As such, graphically, the lines corresponding to the mean flow velocities 0, 5, 10, and 18 in Fig. 5.2, should be stratified from top to bottom respectively, with a similar slope. A portion of Fig. 5.2 was magnified, and is presented in Fig. 5.3. Small changes in the acoustic travel times can be seen, with the average travel time data stratified from top to bottom with increasing flow velocity, as described previously. A bar graph representation of the data presented in Fig. 5.4 also illustrates small changes in the average travel times. It can be seen that the red bar, which denotes data collected at U = 0m/s, is the longest bar in

each grouping, and the pink bar, representing U = 18m/s data, is the shortest. At x/M = 36 the average travel time for U = 18m/s is larger than expected. However, observation of the corresponding data presented in Table 5.1 and in the larger data set confirms the presence of an outlying data point, which has heavily influenced the average travel time. This result can be expected, as statistically, the average is sensitive to outliers (Petruccelli, 1999). These small changes, observed graphically in Fig. 5.3-4, are in agreement with the values presented in Table 5.1, which show deviations in the third

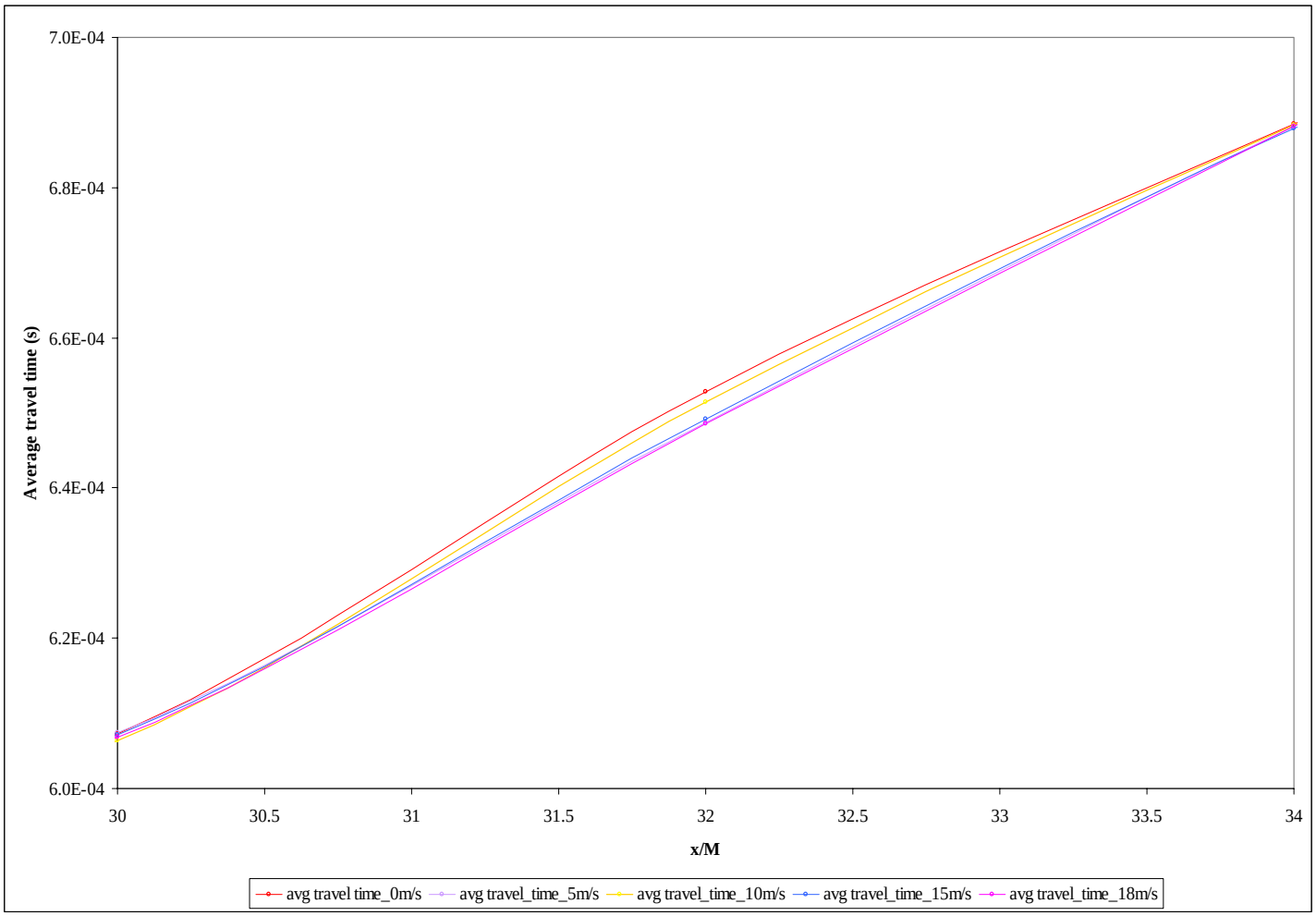

Figure 5-3 - Magnified portion of Figure 5.2

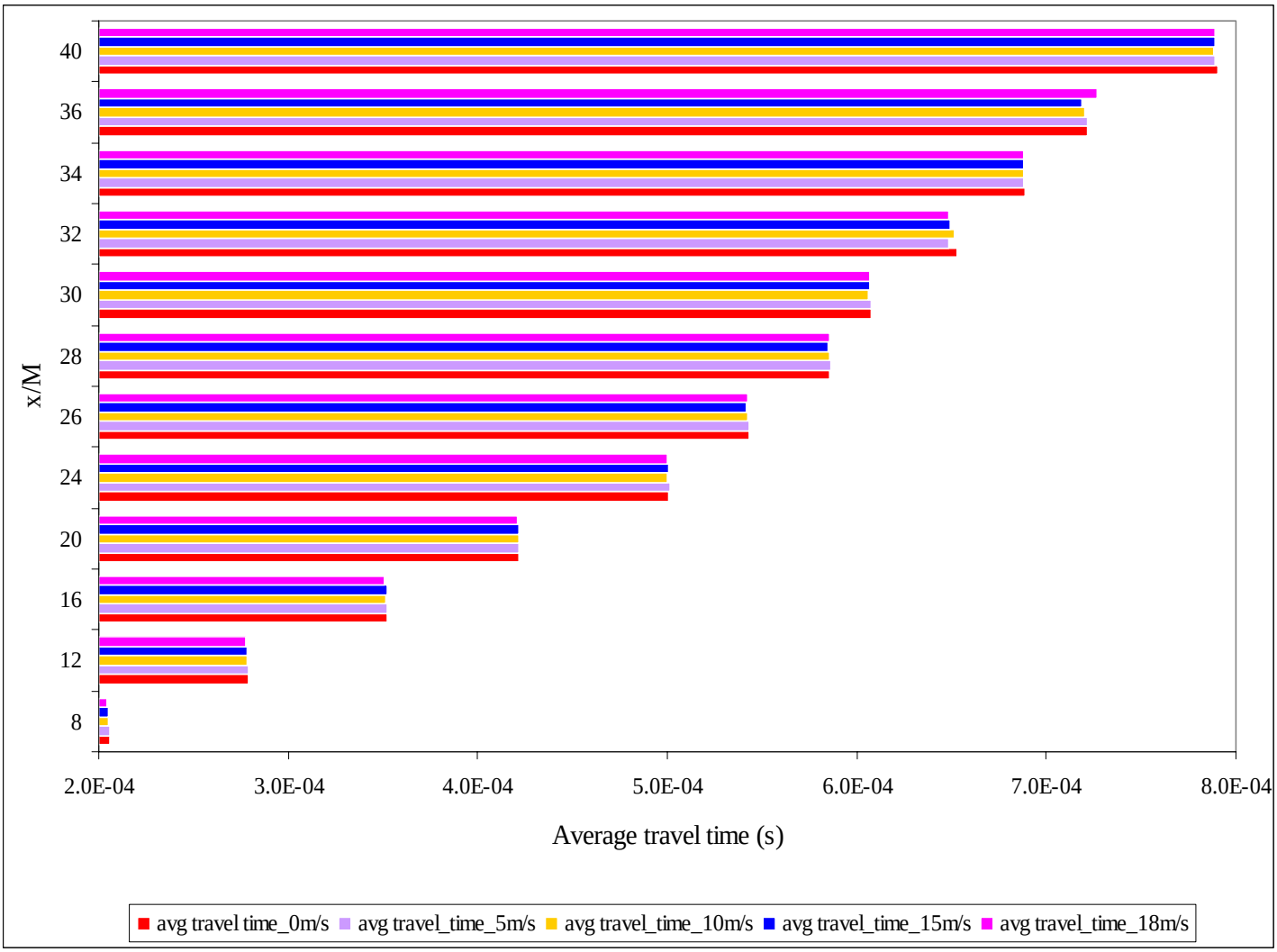

Figure 5-4 - Bar chart representation of mean travel time data 0.25in grid

decimal place. The experiment was also performed using a 0.5in grid, and that data pertaining to the mean travel times is presented in Figure 5.5 and Table 5.2 below.

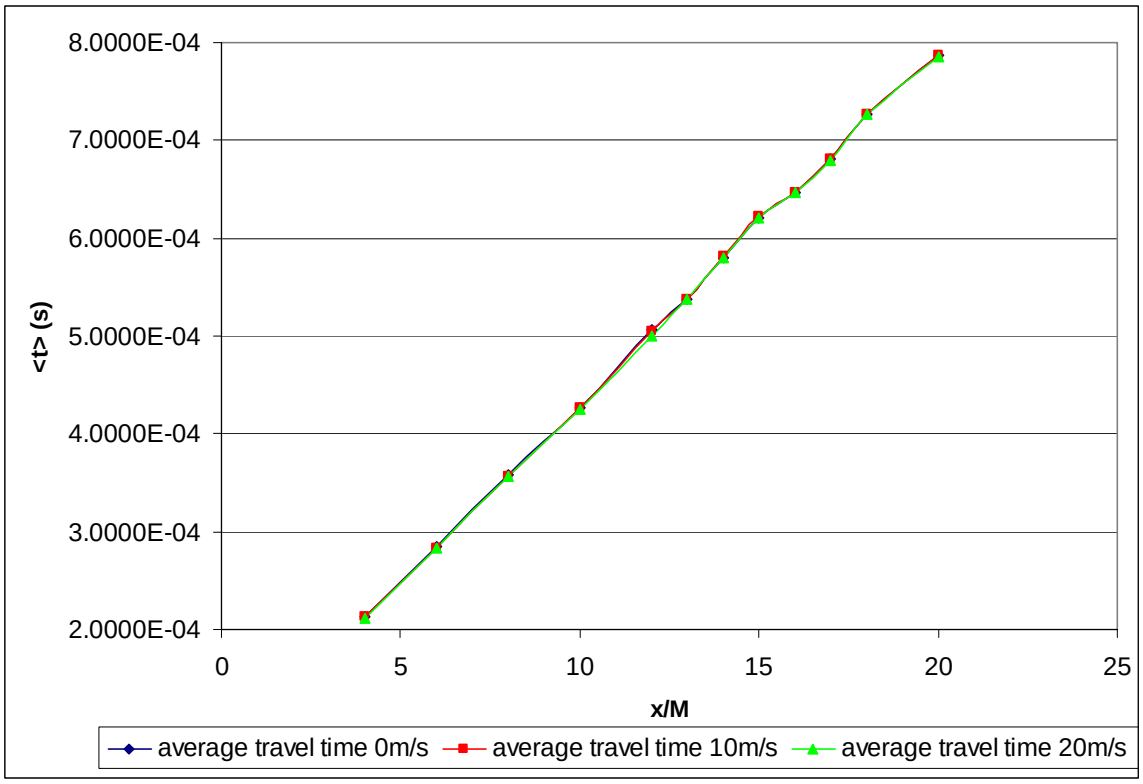

Figure 5-5 - Mean travel time vs. Non-dimensional length scale 0.25in grid

distance x/M	average travel time 0m/s	average travel time 10m/s	average travel time 20m/s
4	2.1309E-04	2.1278E-04	2.1183E-04
6	2.8410E-04	2.8379E-04	2.8295E-04
8	3.5752E-04	3.5713E-04	3.5686E-04
10	4.2685E-04	4.2639E-04	4.2562E-04
12	5.0641E-04	5.0564E-04	5.0081E-04
13	5.3746E-04	5.3709E-04	5.3676E-04
14	5.8046E-04	5.8080E-04	5.7966E-04
15	6.2120E-04	6.2157E-04	6.2100E-04
16	6.4626E-04	6.4667E-04	6.4644E-04
17	6.8064E-04	6.8065E-04	6.8013E-04
18	7.2723E-04	7.2644E-04	7.2600E-04
20	7.8694E-04	7.8662E-04	7.8611E-04

Table 5-2 - 0.5in grid mean travel time table

Similar to the 0.25grid data set, the values in Table 5.2 for the 0.5in grid experiment conducted at mean velocities of 0, 10, and 20 m/s, feature larger changes in the acoustic travel times. Graphically, these changes can be seen in Fig. 5.6-7. The data features changes in the third decimal place, larger than observed in the previous experiment.

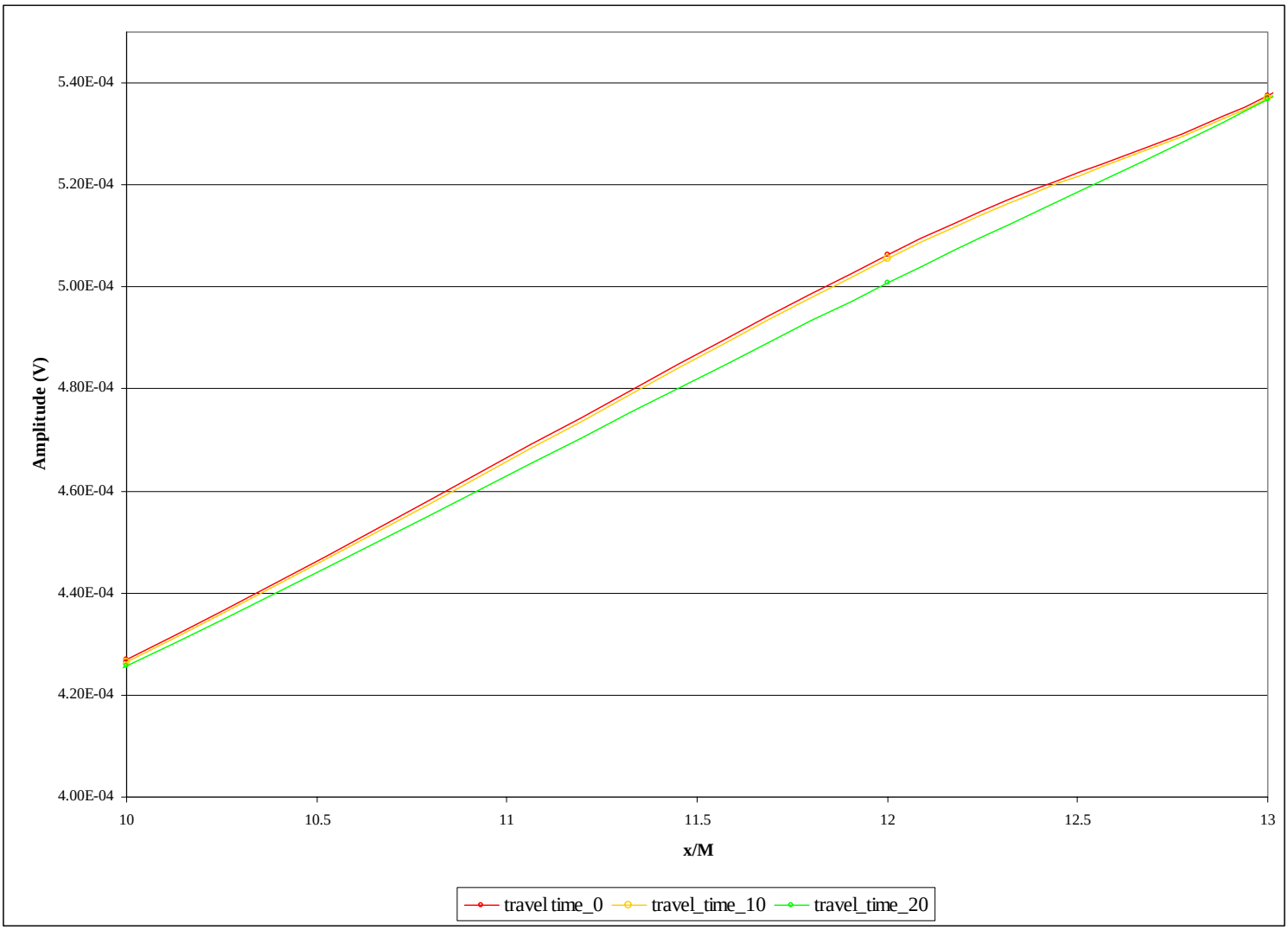

Figure 5-6 - Magnified portion of Figure 5.5

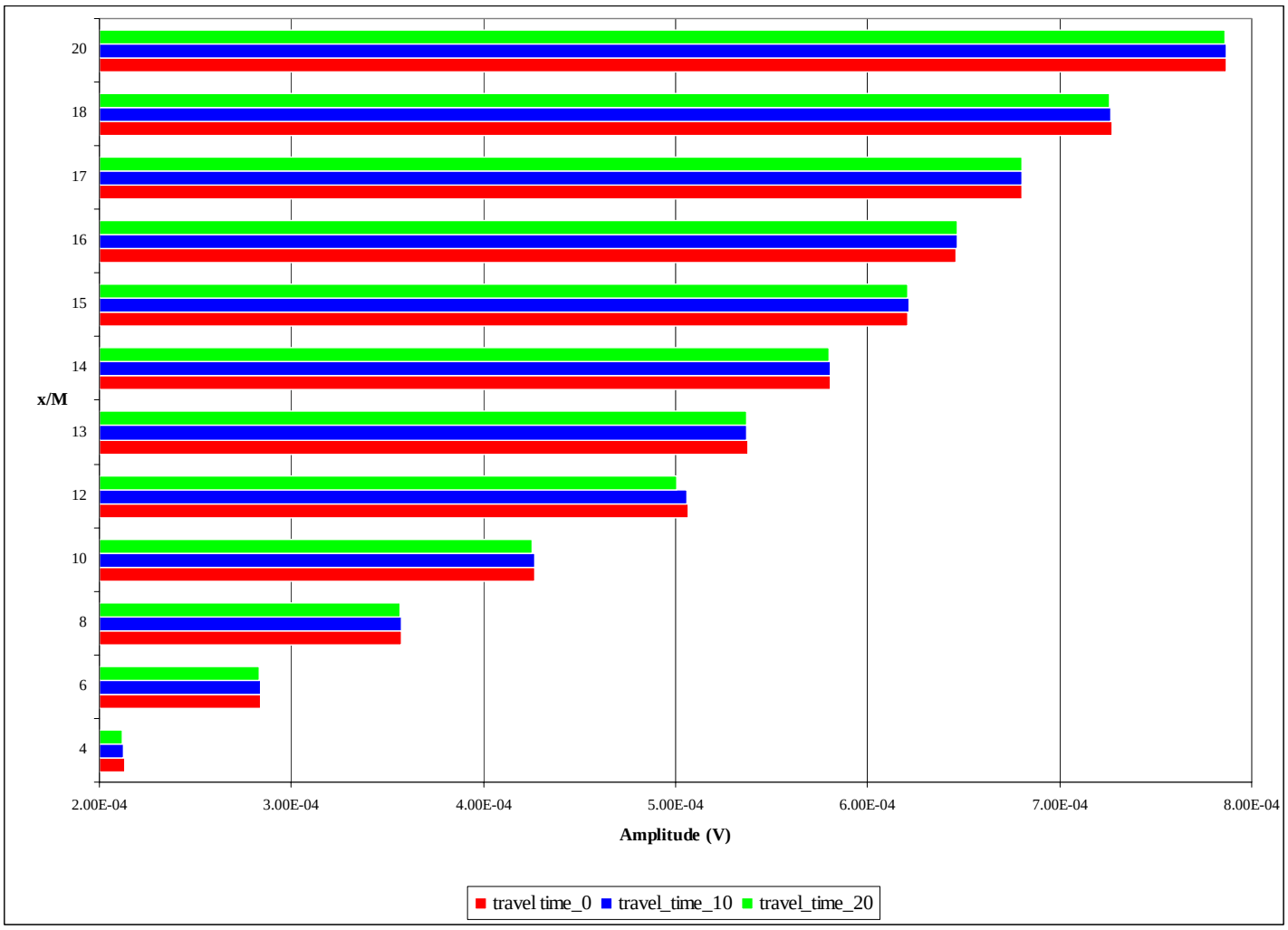

Figure 5-7 - Bar chart representation of mean travel time data 0.5in grid

For comparison, the results of Andreeva and Durgin (2003) are reproduced below for their 1in grid experiment at a mean flow velocity of 3.5m/s in Fig. 5.8. Although their data table is not presented within, the changes in the acoustic travel times present using a 1in grid are appreciably larger than those observed in our study using a 0.25 and 0.5in grid, as they are clearly illustrated in Fig. 5.8. Sound waves propagating through the turbulent atmosphere, an environment that is reasonably comparable to our induced flow conditions, are strongly affected by the large-scale motions of the energy-containing sub-range (Wilson et al., 1998).

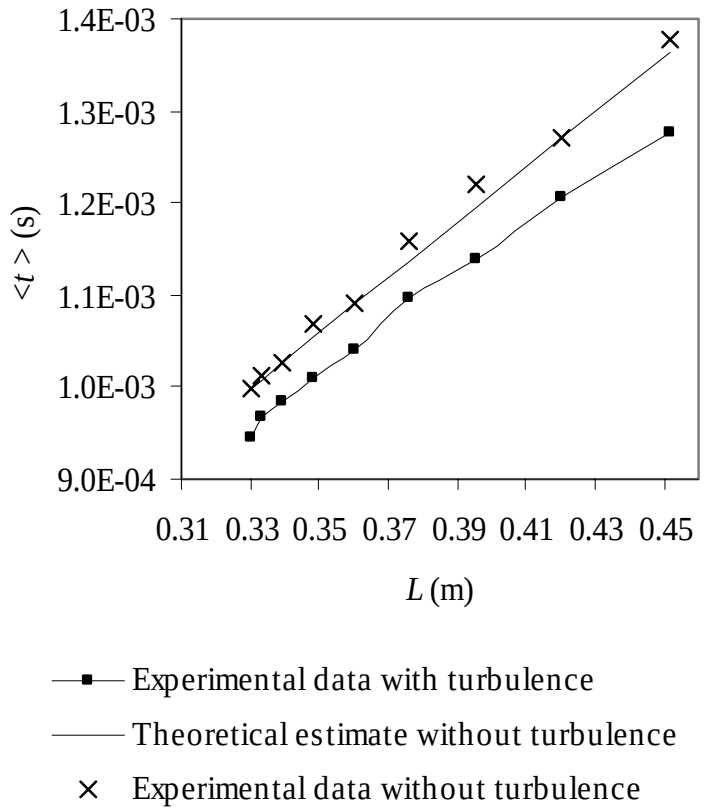

Figure 5-8 - Mean travel time vs. Non-dimensional length scale 1in grid Andreeva and Durgin (2003)

Thus, we can conclude that only the larger turbulent scale inhomogeneities, compared to the wavelength $\lambda = 3 \cdot 10^{-3}$, influence wave propagation and ultimately changes in the acoustic travel time.

5.3 High Amplitude Standard Deviation & Caustic Occurrence

There is a correlation between strong fluctuations of the amplitude of a plane wave in a medium containing large, compared to the wavelength, random inhomogeneities and

the occurrences of the caustics. Obukhov (1953) studied in a quantitative manor the experimental data; mostly collected by Krasilnikov (1949), on amplitude and phase fluctuations of sound and optical waves in turbulent media. Kravtsov (1968) describes wave propagation in such a media using ray theory, as described by Fig. 5.9 reproduced from his works at the USSR Academy of Sciences.

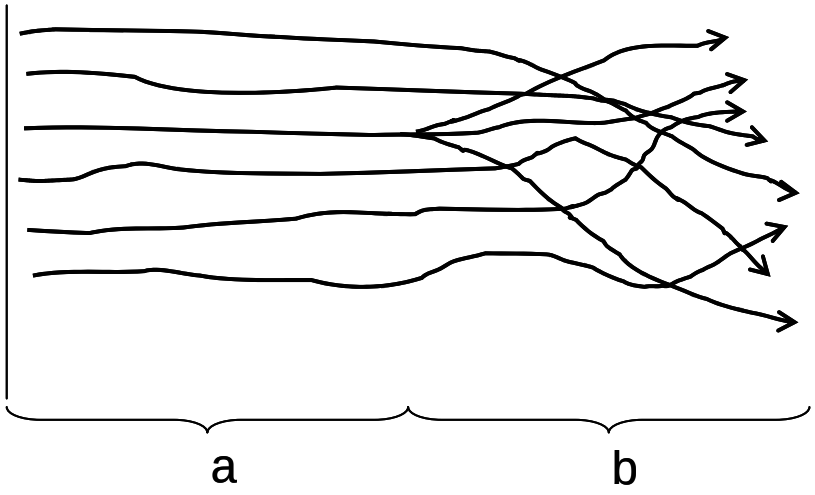

Figure 5-9 - Kravtsov (1968) description of wave propagation through a random medium

In the case of propagation in a randomly inhomogeneous medium, each ray represented in region *a* of the illustration above, experiences random deviations and moves on the average farther away from its initial direction, in accordance with diffusion a law (Kravtsov, 1968). The individual rays can intersect and cause caustics, as shown schematically in region *b* of Fig. 5.9. With the appearance of the caustics, fluctuations in wave amplitude are expected to increase as a result of the "swelling" of the field on the caustics, the formation of the caustic shadow, and of the interference of the waves ahead of the caustic (Kravtsov, 1968). We can therefore expect to observe larger fluctuations of

the wave amplitudes in region *b* of Fig. 5.9 than in region *a* which is free of caustics (Kravtsov, 1968).

Amplitude standard deviations calculated for the 0.5in grid experiment at mean velocities of 0, and 20m/s are presented in Figure 5.10 below, along with comparable data for the 0.25in grid case at 20m/s.

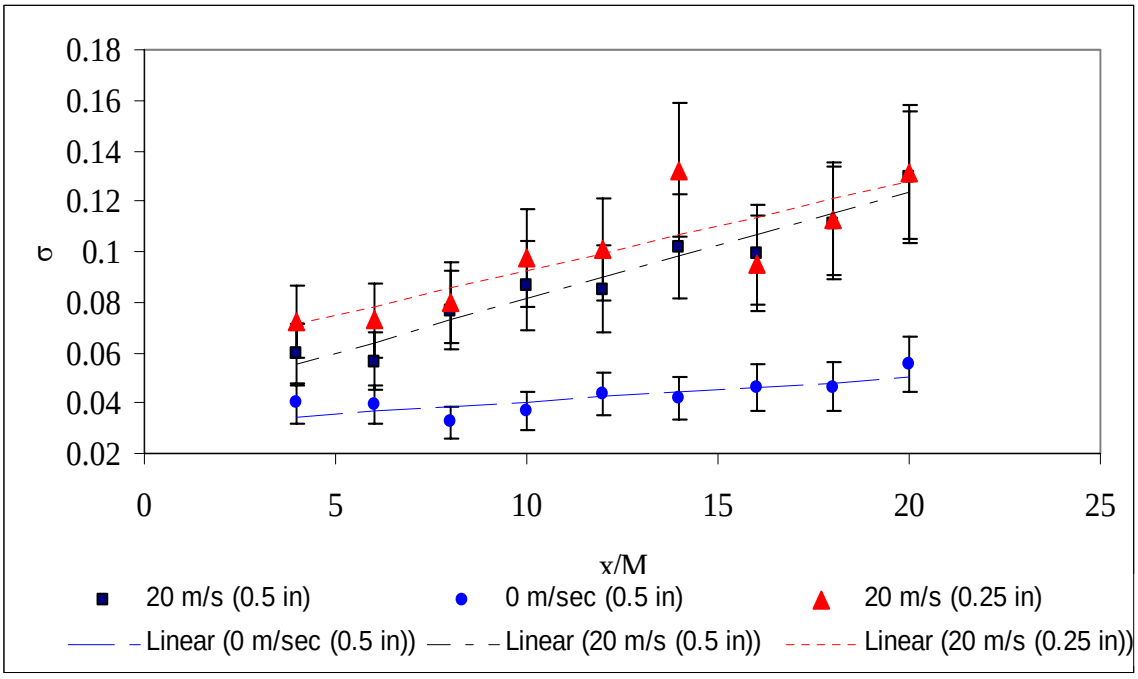

Figure 5-10 - Amplitude standard deviations

From Fig. 5.10, we observe an increase in amplitude fluctuations with increasing non-dimensional lengths, with prominent increases beginning around x/M = 10. We believe that these regions of large amplitude fluctuations correspond to the occurrence of the caustics.

5.4 Travel time Variance & Caustic Occurrence

In similar studies, a link between non-linear trends of the acoustic travel time variance and the occurrence of the first caustics has been made by Iooss et al. (2000). Furthermore, Benon et al. (1995) concluded that for the same variances of sound speed and velocity fluctuations, caustics appear in a purely moving random medium at shorter distances than a purely motionless medium. Moving inhomogeneities disturb the phase front of a sound wave to a greater extent than motionless inhomogeneities (Benon, et al., 1995). It has also been observed that the more disturbances there are in a wave front, the shorter the distance is of the caustic formation (Benon, et al., 1995).

The data corresponding to the measured acoustic travel time variances are presented below in Fig. 5.11-12, for the 0.25in and 0.5in grid experiments respectively. The data presented in Fig. 5.11 show linear increases in the acoustic travel time variance with increasing propagation distance for mean flow velocities of 0, 5, 10, and 15m/s. These data sets complement the Chernov (1960) prediction of linearity in the acoustic travel time variance. The remaining data for mean flow velocities of 18m/s feature an initial linear increase in travel time variance, followed by a non-linear trend initiated at a certain propagation distance. These data sets support the Iooss (2000) prediction of non-linearity in the acoustic travel time variance. We believe this non-linear trend is due to the occurrence of the caustics.

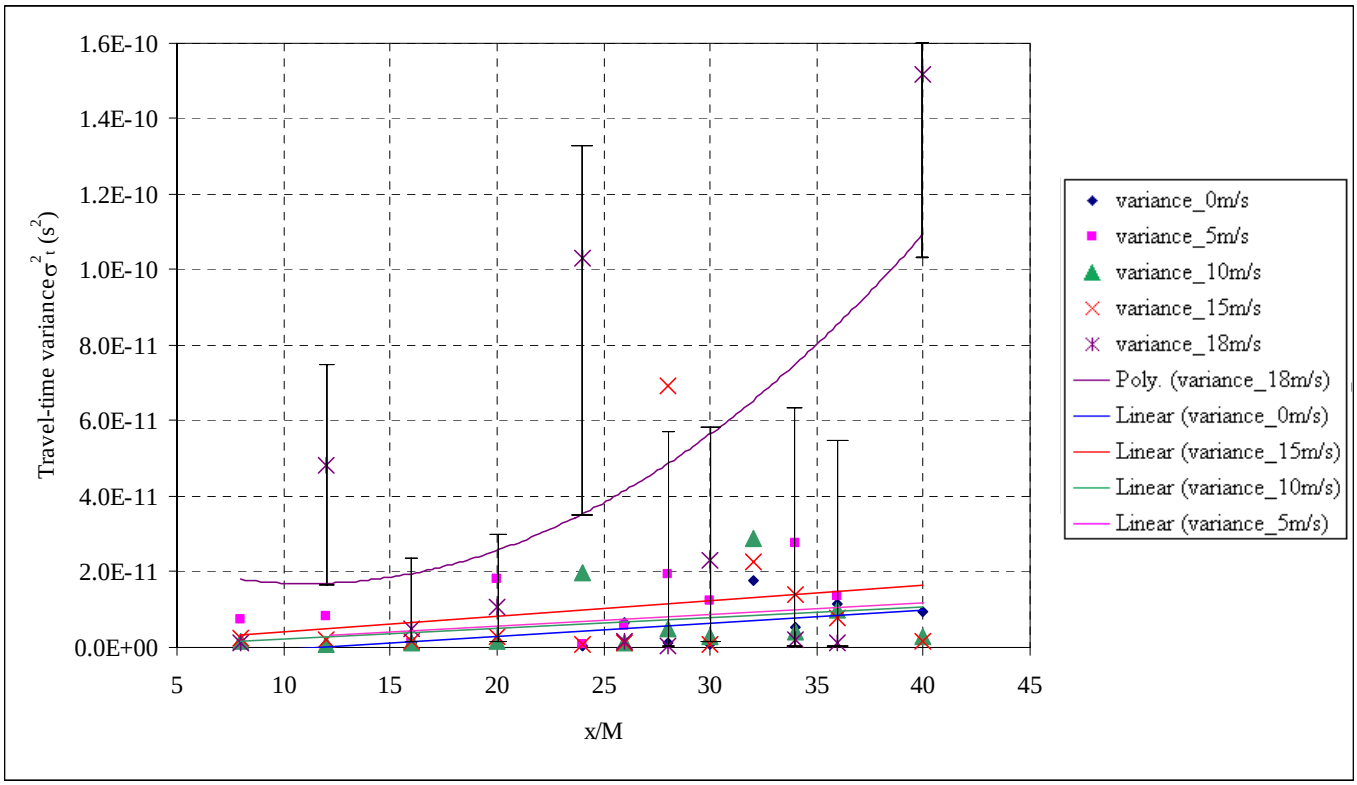

Figure 5-11 - Travel time variance 0.25in grid experiment

The data presented in Fig. 5.12 for the 0.5in grid experiment, for mean flow velocities of 0, 10, and 20 m/s, is plotted over the Iooss (2000) non-linear approximation. These data sets exhibit similar trends as observed above in Fig. 5.11. It can be seen that for U = 0m/s there is a linear increase in the travel time variance. The data collected for U = 10m/s, at lower values of x/M, can be described by a linear increase as well. At larger propagation distances, around x/M = 12, the data departs from a linear increase and follows a non-linear trend. The data collected at U = 20 m/s strongly follows the non-linear increase predicted by Iooss (2000) in the acoustic travel time variance; with our data points falling directly above and below the trend line. Iooss et al. (2000) and

Karweit et al. (1991) observed that the non-linearity effects illustrated in Fig.5.11-12 appear at shorter distances and increase much faster in the plane wave case than in the spherical wave case, for x/M << 35.

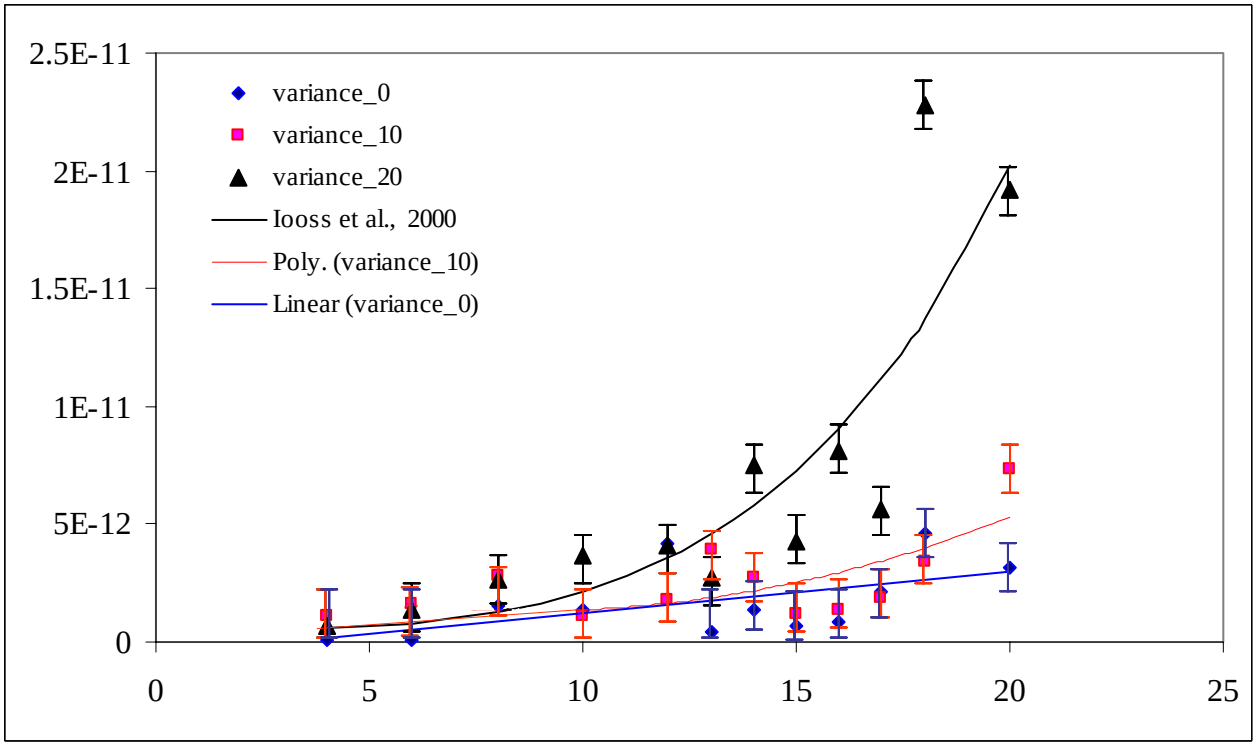

Figure 5-12 - Travel time variance 0.5in grid experiment

In addition, Iooss et al. (2000) validates these non-linear trends numerically, based on random fields generated using random Fourier modes and the Gaussian beam summation to calculate the acoustic field propagated in the medium. Hence, the Gaussian beam approach is used to solve the wave equation in the neighborhood of the conventional rays using the parabolic approximation (Iooss et al., 2000).

The regions corresponding to larger amplitude fluctuations presented in Fig. 5.10 (x/M = 10-15) also coincide with the first instances of non-linear effects in the acoustic

travel time variance plots presented in Fig. 5.11-12. Thus, we can assume from the data that there is some correlation between larger amplitude fluctuations and possible formation of the caustics.

Chapter 6. Conclusions and Recommendations

In this work we have highlighted the pertinent issues which influenced our experimental investigation on non-linear effects in relation to the formation of caustics. The collected and analyzed data from several experiments were presented for the case of a 0.25in and 0.5in welded wire mesh grid turbulence generators for multiple velocities. These results, to a large degree, appeared as initially expected, and are in agreement with comparable experimental and numerical investigations. In the remainder of this section, we will summarize our findings, and define unresolved areas of interest that may lead to future study.

6.1 Summary and Conclusions

Experimental data was presented to examine acoustic travel time variation with increasing ultrasonic path lengths and changing mean velocity. The experiment was preformed for multiple mean flow velocities of 0, 5, 10, 18, and 20 m/s. The ultrasonic path lengths were incrementally increased from 2 – 10 inches. The turbulent intensity for the 0.25 and 0.5in grid experiments was not really strong enough to demonstrate Fermat's principle. A comparison between our experimental data, and similar data collected by Andreeva and Durgin (2003), support the conclusion that only the larger turbulent scale inhomogeneities (compared to the wavelength $\lambda = 3 \cdot 10^{-3}$) influence wave propagation,

and ultimately changes in the acoustic travel time. As a result, only the plot generated from the 1” grid experiment effectively illustrated Fermat’s principle.

The acoustic travel time variance data clearly showed the non-linear behavior of the variance as predicted. Instances of non-linearity appeared at shorter propagation distances as the turbulent intensity was increased. Likewise, Benon et al. (1995) observed the first instances of the non-linearity in the acoustic travel time variance to be shorter for higher flow velocities. Thus, we can conclude as the turbulent intensity is increased, there are more disturbances in a wave front; and the formation of the caustics is realized at increasingly shorter distances. For instances of low turbulent intensity, our data complements the Chernov (1960) prediction of linearity, while data collected at higher turbulent intensities compliment the non-linear prediction of Iooss (2000). Additionally, the non-linear trends in our variance data were validated by comparable numerical work formulated by Iooss et al. (2000), who achieved similar results.

The collected data was also used to compute the amplitude standard deviations. Regions of large amplitude fluctuations also coincided with the first instances of non-linearity in the acoustic travel time variance. Obukhov (1953) and Kravtsov (1968) made the connection between large amplitude fluctuations and the occurrence of the caustics. Our amplitude standard deviation data is in agreement with their predictions; supporting the hypothesis that areas of caustic formation can be predicted by amplitude fluctuations in the region.

6.2 Recommendations

1. The ultrasonic travel time data, collected under very good experimental conditions, could be refined through improvements to the data acquisition system. Specifically,

- The addition of an "independent" external support system to mate with the existing experimental apparatus would confine mechanical vibrations to wind tunnel structures.
- Modification of Gage Sample.vi DAQ control program to support sampling of temperature data.
- An additional CompuScope 82G DAQ board used a slave to enable simultaneous data collection on four channels.

2. Experimental characterization of the turbulent flow field, through hot wire anemometry, would further validate the flow assumptions made in this study based on Mohammed and LaRue (1990).

3. Computation of the probability density function for similarly conducted experiments should yield information specific to the predicted region of caustic formation when viewed in the context of acoustic travel time variance data.

4. Additional experiments using similar grid mesh sizes conducted at angular orientations $\left(\beta \neq 90^{0}\right)$ could be done to complement the work presented within, and detect non-linear behavior in the acoustic travel time variance at larger propagation distances.

Bibliography

Anderson, J. D. *Fundamentals of Aerodynamics: second edition*. New York: McGraw-Hill, 1991.

Andreeva, T. A., Meleschi, S. B., and Durgin, W. W. "Experimental Investigation of Statistical Moments of Travel Time in Grid-Generated Turbulence." *American Institute of Aeronautics and Astronautics*, Vol. 78. 2004: 1-5.

Andreeva, T. A. "Ultrasonic Technique in Determination of Grid-Generated Turbulent Flow Characteristics." *Worcester Polytechnic Institute*, Worcester, 2003: 1-123.

Baldock, G. R., Bridgeman, T. *Mathematical Theory of Wave Motion*. New York: John Wiley & Sons, 1981.

Bendat, Julius S. *Engineering applications of correlation and spectral analysis*. New York: Wiley, 1980.

Blanc-Benon, Ph., Juvé, D., Ostashev, V. E., and Wandelt, R., "On the appearance of caustics for plane sound wave propagation in moving random media." *Waves in Random media*, Vol. 5. 1995: 183-199.

Chernov, L. A. *Wave Propagation in a Random Medium*. New York: McGraw-Hill, 1960.

Emmanuel P. Papadakis., ed. *Ultrasonic instruments and devices: reference for modern instrumentation, techniques, and technology*. California: Academic Press, 1999.

Frisch, U. *Turbulence: the legacy of A.N. Kolmogorov*. Cambridge: Cambridge University Press, 1995.

Gooberman, G. L. *Ultrasonics: theory and application*. London: English Universities P., 1968.

Hinze, J. O. *Turbulence*. New York: McGraw-Hill, 1959.

Iooss, B., Ph., Blanc-Benon, and Lhuillier, C., "Statistical moments of travel times at second order in isotropic and anisotropic random media." *Waves Random Media*, Vol. 10. 2000: 381-394.

Ishimaru, Akira. *Wave propagation and scattering in random media*. New York: Academic Press, 1978.

Johari, H., and Durgin, W. W. "Direct Measurements of Circulation Using Ultrasound." *Experiments in Fluids*, Vol. 25. 1998: 445-454.

Kravtsov, Y. A. "Strong Fluctuations of the Amplitude of a Light Wave and Probability of Formation of Random Caustics." *Soviet Physics Jetp*, Vol. 28, No. 3. 1969: 413-414.

Lighthill, M. J., Sir. *Waves in fluids*. Cambridge: Cambridge University Press, 1978.

Lynnworth, L. C. *Ultrasonic Measurements for Process Control*. San Diego: Academic Press, 1989.

Mohamed, M. S., and La Rue, J. C. "The Decay Power Law in Grid-Generated Turbulence." *Journal of Fluid Mechanics*, Vol. 219. 1990: 195-214.

Montgomery, D. C. *Design and Analysis of Experiments: 5th edition*. New York: John Wiley & Sons, 2001.

Nye, J. F. *Natural Focusing and Fine Structure of Light: Caustics and Wave Dislocations*. United Kingdom: University of Bristol, 1999.

Panton, R. L. *Incompressible Flow: second edition*. New York: John Wiley & Sons, 1996.

Petruccelli, J., Nandram, B., and Chen, M. *Applied Statistics*. New York: Prentice Hall, 1999.

Richardson, Edward Gick. *Ultrasonic physics*. New York: American Elsevier Pub. Co., 1962.

Ristic, Velimir M. *Principles of acoustic devices*. New York: Wiley, 1983.

Rizzoni, Giorgio. *Principles and Applications of Electrical Engineering: third edition*. New York: McGraw-Hill, 1983.

Samuelides, Y., "Velocity shift using the Rytov approximation," *Journal of Acoustical Society of America*, Vol. 104, 1998: 2596-2603.

Schmidt, D. W. "Acoustical Method for Fast Detection and Measurement of Vortices in Wind Tunnels." *ICIASF Record*. 1975: 216-228.

Shiavi, Richard. *Introduction to applied statistical signal analysis*. San Diego: Academic Press, 1999.

Spiesberger, J.L., "Ocean Acousitc Tomography: Travel Time Biases," *Journal of Acoustical Society of America*, Vol. 77. 1985: 83-100.

Sreenivasan, K. R., Tavoularis, S., Henery, R., and Corrsin, S. "Temperature Fluctuations and Scales in Grid-Generated Turbulence." *Journal of Fluid Mechanics*, Vol. 100. 1980: 597-621.

Tatarskii, V. I. "A commentary on A. M. Obukhov's paper: Sound and Light Propagation in a Weakly Inhomogeneous Atmosphere." *Waves in Random media*, Vol. 1. 1994: 7-8.

Tatarskii, V. I. *Wave propagation in a turbulent medium*. New York: McGraw-Hill, 1961.

Yeh, T. T., and Van Atta, C. W. "Spectral Transfer of Scalar and Velocity Fields in Heated-Grid Turbulence." *Journal of Fluid Mechanics*, Vol. 58. 1973: 233-261.

Wilson, K. D., Brasseur, J. G., and Gilbert, K. E. "Acoustic Scattering and the Spectrum of Atmospheric Turbulence." *Journal of Acoustical Society of America*, Vol. 105. 1999: 30-34.

Appendix A – CompuScope 82G Software Interface

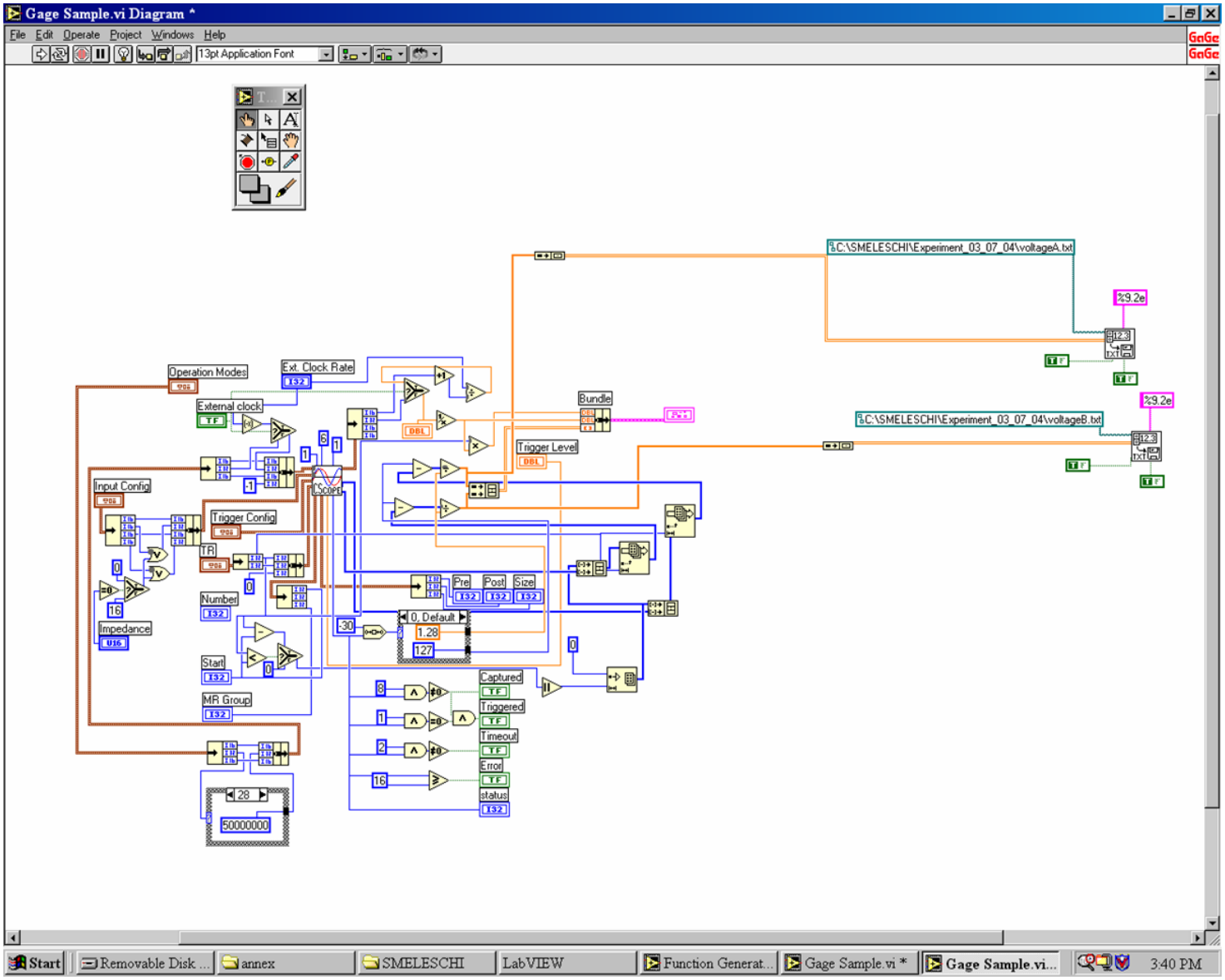

Figure i – CSScope.vi & Gage Sample.vi

Appendix B – IMSL Fortran Signal Correlation Program

```
!The program calculates correlation function to find
! the time interval between the sent and arrived signals

        include '../Input/param.txt'

       INTEGER    IPRINT, MAXLAG, K, NF, LL
    PARAMETER  (IPRINT=0, MAXLAG=1000, NOBS=1024)
    INTEGER    IMEAN, ISEOPT, NCOL, NROW
       REAL                 CC(-MAXLAG:MAXLAG),   CCV(-MAXLAG:MAXLAG),
Y(NOBS),
   &          RDATA(1000,2), SECC(-MAXLAG:MAXLAG),XMEAN,
   &          XVAR, YMEAN, YVAR, X(NOBS)
    double precision XX(N),YY(N),TT(N)
       EXTERNAL   CCF

       kk=1
       ikl=1
!This part of the program opens two files, reads data, makes one file with
!a proper time interval and calculates length of each vectors

!FILE NAMES HAVE TO BE CHANGED/\/\/\/\/\/\/\/\/\/\/\/\/\/\/\/\/\/\/\/\/\/\/
c          open(unit=3,file='../INPUT/TRDPR/DATA/
c    +A_10.txt',status='old')
c          open(unit=5,file='../INPUT/TRDPR/DATA/
c    +B_10.txt',status='old')

c        if (ikl.eq.1) then
c          open(unit=6,file='../INPUT/TRDPR/COM/
c    +AB_10.txt', status='unknown')
           open(unit=7,file='
   +corel.txt', status='unknown')
c        endif
**************************************************************
c        ____________________________________________________________
c        if (kk.eq.1) then
c          open(unit=9,file='../INPUT/RoomTemp/
c    +/Correlation/realcor_10.txt', status='unknown')
c        endif
c        ____________________________________________________________

c          open(unit=10, file='../INPUT/Dt(v)500/
```

```
c    +Amplitude/MAX_Amp_35.txt', status='unknown')
c        write(10,*)'   Max_Send            Max_Received '
!THE LAST FILE IS THE ONE WITH PROPER TIME AND TWO COLUMNS OF
DATA
!/\/\/\/\/\/\/\/\/\/\/\/\/\/\/\/\/\/\/\/\/\/\/\/\/\/\/\/\/\/\/\/\/\/\/\


c          do i=1,N
c          read(3,*,end=2) TT(i),YY(i)
c          end do
c  2       continue
c          do i=1,N
c          read(5,*,end=4) TT(i),XX(i)
c          end do
c  4       continue

c          do j=1,N
c          TT(j)=TT(2)*(j-1)
**************************************
c        print*,'TT=',TT(2),TT(j)
c        if (TT(2).GT.1.e-5) then
c        print*,'j=',j
c        endif
**************************************

c        if (ikl.eq.1) then
c          write(6,8)TT(j),XX(j),YY(j)
c  8       format(3x,3(E15.6,3x))
c        endif
c          enddo
c          close(3)
c          close(5)
c          close(6)
!/\/\/\/\/\/\/\/\/\/\/\/\/\/\/\/\/\/\/\/\/\/\/\/\/\/\/\/\/\/\/\/\/\/\/\/
!/\/\/\/\/\/\/\/\/\/\/\/\/\/\/\/\/\/\/\/\/\/\/\/\/\/\/\/\\/\/\/\\/\/\/
         PI = 4.*atan(1.)
         IMEAN = 1
    ISEOPT = 0
!================================================================
======
! This block selects a data interval from all data
c         NF=N/NOBS
c         do LL=1,NF

!================================================================
=======
```

```
c         do J=NOBS*(LL-1)+1,LL*NOBS
c          X(-NOBS*(LL-1)+J)=1.*XX(J)
c          Y(-NOBS*(LL-1)+J)=1.*YY(J)
c         end do

          CALL CCF (NOBS, X, Y, MAXLAG, IPRINT, ISEOPT, IMEAN, XMEAN,
     &         YMEAN, XVAR, YVAR, CCV, CC, SECC)

c         S=0.
          print*,XMEAN, YMEAN
          do I=1,2*MAXLAG+1
c
c         if (CC(I).GE.S) then
c                 S=CC(I)
c                 K=I
c         endif
c         if (kk.eq.1) then
          write(7,*)(I-1)*0.1*PI,CC(I)
c         endif
          end do
c         write(7,*)'delta_T',K*TT(2)

          sum=0
          do I=1,1024
          sum=sum+Y(I)
          enddo
          averageY=sum/1024.

          smaxX=0.
          smaxY=0.

          do I=1, 1024
          if (abs (X(I)).GT.smaxX) then
          smaxX=abs(X(I))
          endif
          if (abs  (Y(I)-averageY).GT.smaxY) then
          smaxY=abs(Y(I)-averageY)
          endif
          end do
          write (10,*)smaxX,smaxY
c         end do
          end


Make sure your input files are in ../Input/*.* directory!
!=========================================================
```

```
      open(unit=3,file='../INPUT/TRDPR/DATA/
     +A_10.txt',status='old')
      open(unit=5,file='../INPUT/TRDPR/DATA/
     +B_10.txt',status='old')
      open(unit=4,file='../INPUT/param.txt', status='unknown')

      i=1
1     read(3,*,end=10) t,t
      i=i+1
      goto 1
10    N1=i
      j=1
2     read(5,*,end=20) t,t
      j=j+1
      goto 2
20    N2=j
      if (N1.lt.N2) then
      N=N1
      else
      N=N2
      endif
      Print*,'N=',N
      write(4,5)N-1
5     format('      PARAMETER (N=',I8,')')

      write(*,*)'File "param.txt" has been successfully created'
      close(3)
      close(4)
      close(5)
      end
```

Appendix C – Photographs of Experimental Apparatus

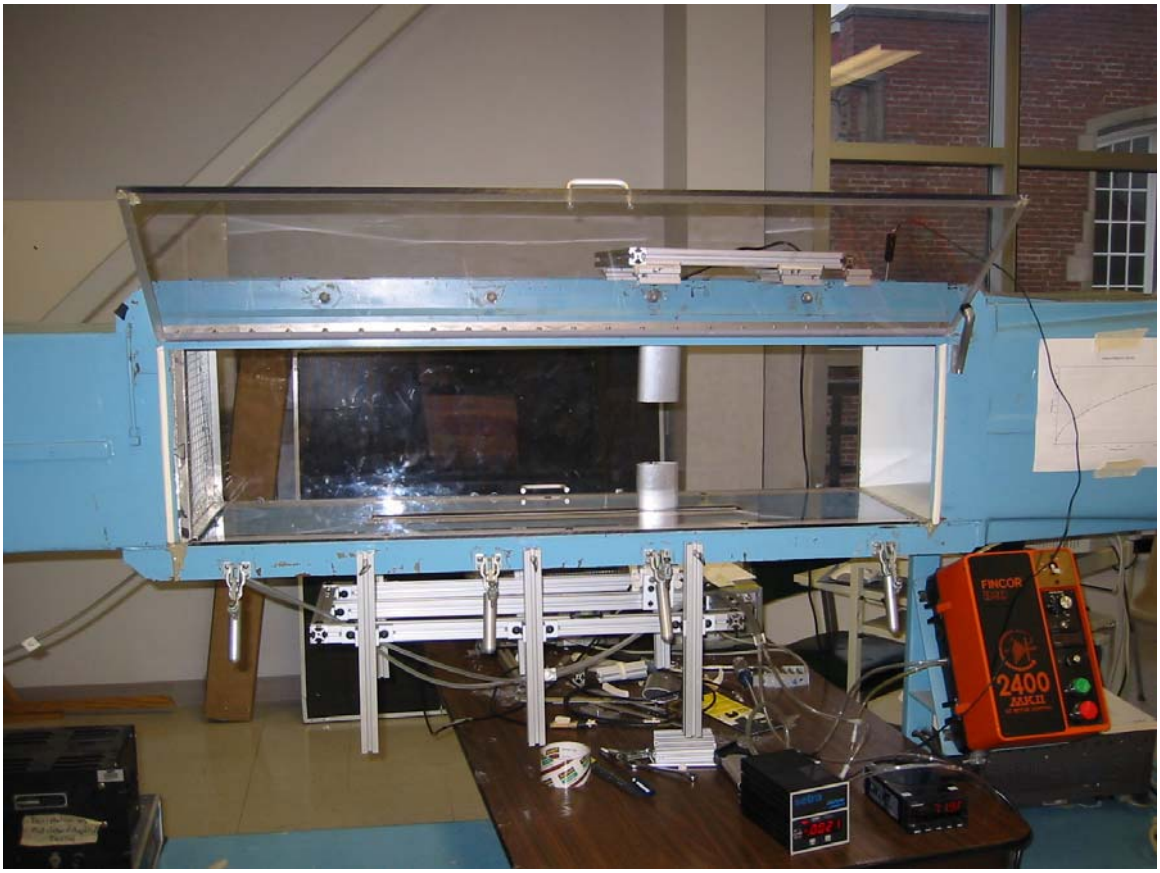

Figure ii - Wind tunnel test section and experimental apparatus

Figure iii – (left to right) Function Generator and Oscilloscope

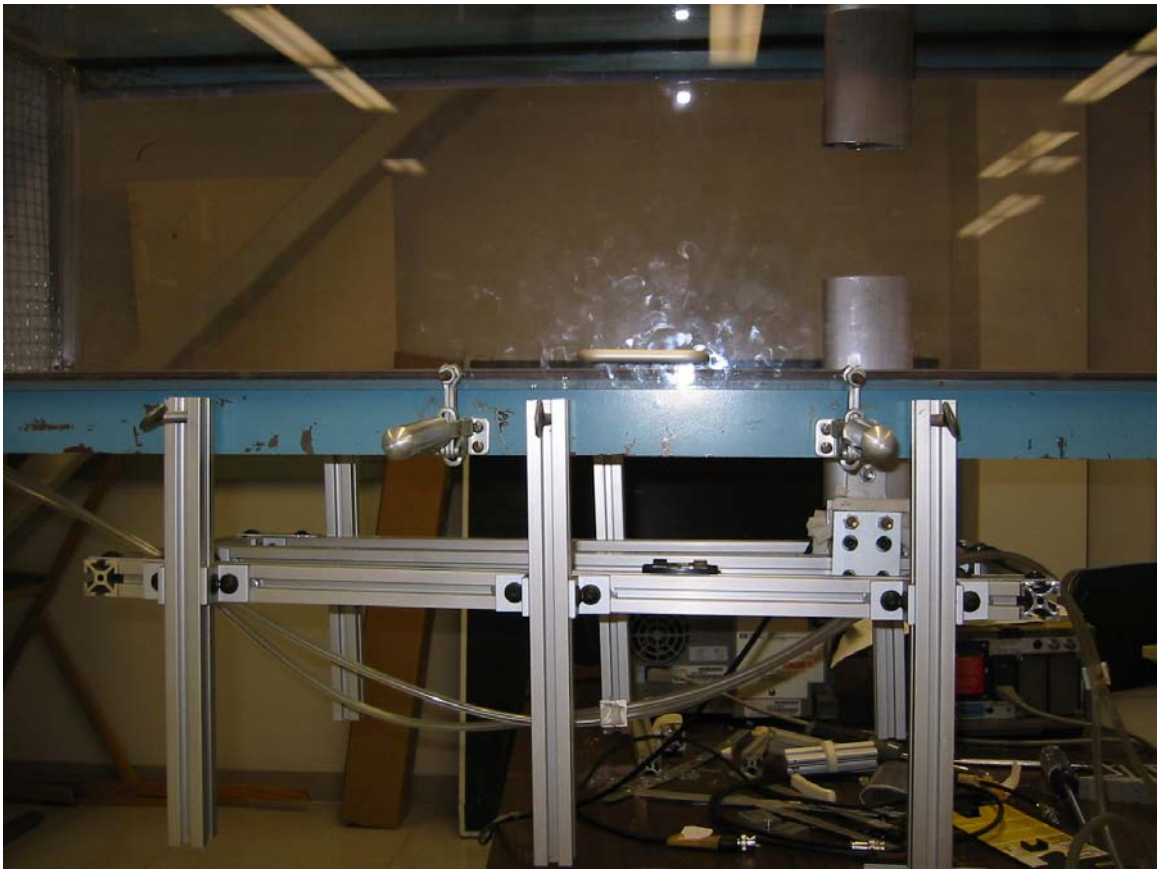

Figure iv - Close-up of supporting apparatus